

WL-TR-93-3048

NUMERICAL SIMULATION OF TRANSIENT
VORTEX BREAKDOWN ABOVE A PITCHING DELTA WING

AD-A281 075



MIGUEL R. VISBAL
COMPUTATIONAL FLUID DYNAMICS RESEARCH BRANCH
AEROMECHANICS DIVISION

MAY 1993

FINAL REPORT FOR 01/01/92-12/31/92

APPROVED FOR PUBLIC RELEASE; DISTRIBUTION IS UNLIMITED.

DTIC
SELECTED
JUL 06 1994
S B D

FLIGHT DYNAMICS DIRECTORATE
WRIGHT LABORATORY
AIR FORCE MATERIEL COMMAND
WRIGHT PATTERSON AFB OH 45433-7562

DTIC QUALITY INSPECTED 3

3P8 94-20443



94 7 5 092

NOTICE

When Government drawings, specifications, or other data are used for any purpose other than in connection with a definitely Government-related procurement, the United States Government incurs no responsibility or any obligation whatsoever. The fact that the government may have formulated or in any way supplied the said drawings, specifications, or other data, is not to be regarded by implication, or otherwise in any manner construed, as licensing the holder, or any other person or corporation; or as conveying any rights or permission to manufacture, use, or sell any patented invention that may in any way be related thereto.

This report is releasable to the National Technical Information Service (NTIS). At NTIS, it will be available to the general public, including foreign nations.

This technical report has been reviewed and is approved for publication.

Miguel Visbal

MIGUEL VISBAL
Aerospace Engineer
CFD Research Section

Joseph Manter

JOSEPH MANTER
Chief
CFD Research Branch

Dennis Sedlock

DENNIS SEDLOCK
Actg Chief
Aeromechanics Division

If your address has changed, if you wish to be removed from our mailing list, or if the addressee is no longer employed by your organization please notify WL/FIMC, WPAFB, OH 45433-7562 to help us maintain a current mailing list.

Copies of this report should not be returned unless return is required by security considerations, contractual obligations, or notice on a specific document.

REPORT DOCUMENTATION PAGE

Form Approved
OMB No. 0704-0188

Public reporting burden for this collection of information is estimated to average 1 hour per response, including the time for reviewing instructions, searching existing data sources, gathering and maintaining the data needed, and completing and reviewing the collection of information. Send comments regarding this burden estimate or any other aspect of this collection of information, including suggestions for reducing this burden, to Washington Headquarters Services, Directorate for Information Operations and Reports, 1215 Jefferson Davis Highway, Suite 1204, Arlington, VA 22202-4302, and to the Office of Management and Budget, Paperwork Reduction Project (0704-0188), Washington, DC 20503.

| | | |
|--|----------------|--|
| 1. AGENCY USE ONLY (Leave blank) | 2. REPORT DATE | 3. REPORT TYPE AND DATES COVERED |
| | 4 May 94 | Final Report Jan 92 - Dec 92 |
| 4. TITLE AND SUBTITLE | | 5. FUNDING NUMBERS |
| Numerical Simulation of Transient Vortex Breakdown Above a Pitching Delta Wing | | PE: 61102F PR: 2307 TA: N6 WU: 11 |
| 6. AUTHOR(S) | | |

Miguel R. Visbal (513) 255-2455

| | |
|--|--|
| 7. PERFORMING ORGANIZATION NAME(S) AND ADDRESS(ES) | 8. PERFORMING ORGANIZATION REPORT NUMBER |
| Flight Dynamics Directorate Wright Laboratory Air Force Materiel Command Wright-Patterson AFB OH 45433-7562 | WL-TR-93-3048 |

| | |
|--|--|
| 9. SPONSORING/MONITORING AGENCY NAME(S) AND ADDRESS(ES) | 10. SPONSORING/MONITORING AGENCY REPORT NUMBER |
| Flight Dynamics Directorate Wright Laboratory Air Force Materiel Command Wright-Patterson AFB OH 45433-7562 | WL-TR-93-3048 |

| | |
|---|------------------------|
| 11. SUPPLEMENTARY NOTES | |
| Completely in-house research submitted for publication in AIAA Journal. | |
| 12a. DISTRIBUTION/AVAILABILITY STATEMENT | 12b. DISTRIBUTION CODE |

Approved for public release; distribution unlimited.

| |
|---|
| 13. ABSTRACT (Maximum 200 words) |
| Computational results are presented for transient vortex breakdown above a delta wing subject to a pitch-and-hold maneuver to high angle of attack. The flows are simulated by solving the full three-dimensional Navier-Stokes equations on a moving grid using the implicit Beam-Warming algorithm. An assessment of the effects of numerical resolution, and favorable comparison with experimental data suggest the computational approach captures the basic dynamics of this transient breakdown. The pressure gradient along the vortex axis is found to play a dominant role in the initiation of breakdown. A description of the three-dimensional instantaneous structure of the flow field is provided for the first time using critical-point theory. The reversed-flow region in the vortex core is associated with pairs of opposite spiral/saddle critical points. At its onset, the vortex breakdown is fairly axisymmetric; however, as it proceeds upstream and a stronger transition takes place along the axis, asymmetric effects become important and result in the formation of a bubble-type breakdown. This bubble structure is open and contains within itself a pair of stagnation points which are diametrically opposed and which rotate in the same sense as the base flow. |

| | | | |
|---|--|---|----------------------------|
| 14. SUBJECT TERMS | 15. NUMBER OF PAGES | | |
| Vortex Breakdown, Delta Wings, Unsteady Aerodynamics, Computational Fluid Dynamics | 42 | | |
| 16. PRICE CODE | | | |
| 17. SECURITY CLASSIFICATION OF REPORT | 18. SECURITY CLASSIFICATION OF THIS PAGE | 19. SECURITY CLASSIFICATION OF ABSTRACT | 20. LIMITATION OF ABSTRACT |
| Unclassified | Unclassified | Unclassified | Unlimited |

Contents

| | |
|--|----|
| Acknowledgments | iv |
| List of Figures | v |
| List of Symbols | vi |
| 1 Introduction | 1 |
| 2 Method of Solution | 3 |
| 2.1 Governing Equations and Numerical Procedure | 3 |
| 2.2 Grid Structure and Boundary Conditions | 3 |
| 2.3 Critical-Point Theory | 4 |
| 3 Results | 6 |
| 3.1 Numerical Resolution Effects | 6 |
| 3.2 Evolution of Transient Breakdown | 7 |
| 3.3 Topology of Sectional Streamlines | 10 |
| 3.4 Three-Dimensional Topology of Vortex Breakdown | 12 |
| 4 Conclusions | 15 |
| 5 References | 16 |

| | |
|---------------------|-------------------------------------|
| Accession For | |
| NTIS GRA&I | <input checked="" type="checkbox"/> |
| DTIC TAB | <input type="checkbox"/> |
| Unannounced | <input type="checkbox"/> |
| Justification | |
| By _____ | |
| Distribution/ _____ | |
| Availability Codes | |
| Dist. | Avail and/or Special |
| P-1 | |

Acknowledgments

I would like to thank Prof. D. Rockwell and Drs. J.-C. Lin and C. Magness for providing the experimental data, and for their kind assistance in its interpretation. Helpful conversations with Dr. R. Gordnier are gratefully acknowledged. Computational resources for this study were provided by the Numerical Aerodynamic Simulation Program (NAS) and by the Air Force Phillips Laboratory, Kirtland AFB, NM.

List of Figures

| | | |
|----|--|----|
| 1 | Critical-Point Concepts | 19 |
| 2 | Effect of Numerical Resolution on Computed Pitching Moment Coefficient | 20 |
| 3 | Effect of Numerical Resolution on Vortex Burst Location | 21 |
| 4 | Effect of Grid Resolution on Axial Velocity in a Vertical Plane Through Vortex Core at $t^+ = 2.14$. (Contours of U'/U_∞ from -3.0 to 3.0 in 0.2 increments) | 22 |
| 5 | Axial Velocity Contours and Velocity Vectors on Plane Through Vortex Core at $t^+ = 1.8, 2.06, 2.26, 2.3, 2.34$ and 2.4 | 23 |
| 6 | Evolution of Axial Velocity Component along Vortex Axis During Transient Breakdown | 24 |
| 7 | Evolution of Pressure Along Vortex Axis During Transient Breakdown | 25 |
| 8 | Comparison of Computed and Experimental [19] Vortex Breakdown Locations | 26 |
| 9 | Comparison of Computed and Experimental [19] Axial Velocity Contours on Plane Through Vortex Core | 27 |
| 10 | Comparison of Computed and Experimental [19] Axial Velocity Profiles Through Breakdown Bubble | 28 |
| 11 | Switch of Azimuthal Vorticity Component, $t^+ = 2.26$ | 29 |
| 12 | Evolution of Crossflow Topology, $t^+ = 2.06$ | 30 |
| 13 | Sectional Streamline Patterns on Vertical Plane Through Breakdown Bubble: (a) Experiment [19], (b) Computed, $t^+ = 2.4$, (c) Computed, $t^+ = 2.6$, (d) Schematic | 31 |
| 14 | Three Dimensional Critical Points and Trajectories in Vortex Breakdown Region at $t^+ = 1.8$ | 32 |
| 15 | Three Dimensional Critical Points and Trajectories in Vortex Breakdown Region at $t^+ = 2.06$ | 33 |
| 16 | Three Dimensional Critical Points and Trajectories in Vortex Breakdown Region at $t^+ = 2.26$ | 34 |
| 17 | Three Dimensional Critical Points and Trajectories in Vortex Breakdown Region at $t^+ = 2.4$ | 35 |
| 18 | Comparison of Computed Results with Experimental [13] Flow Visualization of 'Axisymmetric' Vortex Breakdown in a Tube | 36 |

List of Symbols

| | |
|-----------------|--|
| C | wing chord |
| C_m | pitching moment coefficient about midchord |
| C_p | pressure coefficient, $2(p - p_\infty)/\rho U_\infty^2$ |
| F^+, F^- | stable and unstable foci |
| S^+, S^- | attracting and repelling 3-D spiral/saddle critical points |
| t | time |
| t^+ | non-dimensional time, tU_∞/C |
| u, v, w | velocity components in wing frame of reference |
| U' | axial velocity component |
| U_∞ | freestream velocity |
| X_b | chordwise location of vortex breakdown |
| X, Y, Z | cartesian coordinate system attached to the wing |
| X', Y', Z' | coordinate system attached to wing apex and aligned with vortex axis |
| α | angle of attack |
| Ω | pitch rate, rad/sec |
| Ω^+ | non-dimensional pitch rate, $\Omega C/U_\infty$ |
| ω_θ | azimuthal vorticity component |

1. Introduction

Study of the unsteady aerodynamics of delta wings at high angle of attack is motivated by current interest in enhanced aircraft maneuverability. Ashley et al. [1] have recently reviewed experimental work on delta wings pitching to high incidence. This work shows that during transient high-angle-of-attack maneuvers, a lag in the onset of the leading-edge vortex breakdown occurs [2-4] as compared to a stationary wing. This lag is also accompanied by overshoots in the wing aerodynamic loads [3,5]. The initiation and unsteady behavior of vortex breakdown represents therefore one of the central issues in high-angle-of-attack aerodynamics.

From a more general perspective, vortex breakdown is also observed in swirling flow devices, combustion chambers, trailing vortices and tornadoes. Excellent reviews of experimental and theoretical work on vortex breakdown are given by Hall [6], Leibovich [7,8] and Escudier [9]. These reviews show that despite the significant progress achieved in the characterization of vortex breakdown, more remains to be learned concerning its origin and structure before a comprehensive theory explaining the phenomenon can be established. As suggested by Leibovich and Kribus [10], such a theory must, at a minimum, account for large-amplitude axisymmetric waves, energy transfer to asymmetric modes, and axial pressure gradient effects. Further theoretical developments require systematic experimental and computational studies which describe the instantaneous structure of vortex breakdown. This is particularly true, if active control of breakdown is sought in order to enhance aircraft maneuverability or to alleviate undesirable fluid/structure interactions (e.g. aircraft tail buffet).

The structure of vortex breakdown has been traditionally studied [11-13] using standard flow visualization techniques. Based on the appearance of the streaklines, these experiments point to the existence of two major modes of breakdown, referred to as "spiral" and "bubble" types. Although of great value, these visualizations do not necessarily provide a precise definition of the complex three-dimensional (3-D) instantaneous structure of the flow. For instance, a clear distinction between the spiral and bubble forms of breakdown, based on the actual topology of the velocity or vorticity field, is not presently available. However, it should be noted that measured mean internal bubble structures are given by Falor and Leibovich [14] and Bornstein and Escudier [15]. To overcome the limitations inherent in standard flow visualizations, recent experimental studies [16-20] on vortex bursting above delta wings have concentrated on detailed measurements of the velocity field.

The objective of the present numerical investigation is to describe the unsteady flow structure above a pitching delta wing during the onset and initial stages of transient vortex breakdown. To achieve this goal, calculations are performed for a 75° sweep delta wing

which is pitched at a constant rate to a high angle of attack. Conditions corresponding to the low Reynolds number experiments of Refs. 16 and 19 are selected for the purpose of comparison. The selection of a low Reynolds number (9,200 based on the wing chord) eliminates the uncertainties associated with turbulence modeling and diminishes grid resolution requirements. Nonetheless, as the results will show, this Reynolds number is high enough for non-axisymmetric features to be present, which are considered to be important in any realistic flow displaying vortex breakdown. Furthermore, since the wing is pitched at a high rate, a well defined axial pressure gradient is imposed on the leading-edge vortex. This dominant pressure gradient effect, which arises naturally from the external flow, makes the present configuration more attractive than that of an isolated vortex [21,22], where breakdown is controlled by the specified (and somewhat artificial) boundary conditions.

The flows are simulated by solving the unsteady three-dimensional compressible Navier-Stokes equations on a moving grid using a time-accurate implicit solver which has been previously validated. In this study, only one half of the delta wing is considered, and the flow is assumed to be fully symmetric about the wing centerline. This is done in order to provide better numerical resolution of the breakdown region. The validity of this assumption may be judged *a posteriori* by the good comparison with the experiments. An assessment of the effects of grid resolution on the computed results is presented. Comparisons with experiments [16,19] are provided in terms of the instantaneous vortex breakdown location and flow structure. A characterization of the three-dimensional instantaneous structure of the breakdown region is given for the first time using concepts from critical-point theory [23]. These computational results are also helpful in the interpretation of experimental velocity measurements usually obtained in selected planes through the flow.

2. Method of Solution

2.1 Governing Equations and Numerical Procedure

The governing equations are the unsteady, three-dimensional compressible Navier-Stokes equations written in strong conservation law form [24]. Closure of this system of equations is provided by the perfect gas law, Sutherland's viscosity formula and the assumption of a constant Prandtl number ($\text{Pr} = 0.72$). In order to deal with the case of external flow past a body in general motion, a time-dependent coordinate transformation is incorporated.

The governing equations are numerically solved employing the implicit approximate-factorization Beam-Warming algorithm [25]. The scheme is formulated using Euler implicit time differencing and second order finite-difference approximations for all spatial derivatives. Fourth order explicit and second order implicit damping terms are added to control spurious numerical oscillations [26]. Newton subiterations [27, 28] are also incorporated in order to reduce linearization and factorization errors thereby improving the temporal accuracy and stability properties of the algorithm. A fully vectorized, time accurate, three-dimensional Navier-Stokes solver has been developed using this scheme. The code has been validated for a variety of both steady and unsteady flows, including: flat-plate boundary layers, vortex shedding behind a circular cylinder, dynamic stall of a pitching airfoil [29], Taylor-vortex flow [30], delta wings [28,31], juncture flows [32] and flow past a pitching forebody [33].

2.2 Grid Structure and Boundary Conditions

The computational grid for the flat-plate delta wing is of the H-H type [28] and is obtained using simple algebraic techniques. Two different grids consisting of $98 \times 115 \times 102$ points (Grid 1), and $141 \times 115 \times 118$ points (Grid2) in the ξ , η , ζ directions respectively have been employed in order to assess resolution effects. The ξ , η and ζ directions correspond to the streamwise, spanwise and normal directions relative to the delta wing. For the finer grid, the minimum spacing normal to the wing is $\Delta Z/C = 0.0001$, the spacing along the wing leading edge varies from $\Delta Y/C = 5 \times 10^{-5}$ at the apex to $\Delta Y/C = 5 \times 10^{-4}$ at the trailing edge, and the streamwise spacing on the wing is $\Delta X/C = 0.01$. The far field boundaries for both grids are located two chord lengths away from the delta wing. The effect of far field boundary placement was investigated [34] for an 80° sweep delta wing at 30° angle of attack, and found to be insignificant when the distance from the far field boundary to the wing was increased from 1.5 to 3.0 chord lengths. The boundary conditions are implemented as described in Ref. 28. At the lower, upper, side and upstream boundaries,

characteristic conditions [35] are specified. On the downstream boundary, flow variables are extrapolated from the interior. Symmetry conditions are imposed along the mid-plane of the wing. On the wing surface, the following conditions are applied:

$$\vec{U} = \vec{U}_b \quad (2.1)$$

$$\frac{\partial T}{\partial \zeta} = 0 \quad (2.2)$$

$$\frac{\partial p}{\partial \zeta} = \rho \vec{a}_b \cdot \hat{n} \quad (2.3)$$

where \vec{U}_b and \vec{a}_b denote respectively the surface velocity and acceleration of the pitching wing given by the prescribed motion. For the present computations, a pitch-and-hold maneuver is considered in which the wing accelerates from rest to a constant pitch rate and then decelerates as it reaches its final angle of attack.

2.3 Critical-Point Theory

As noted earlier, one of the objectives of the present study is the description of the unsteady structure of vortex breakdown above the wing. For this purpose, the instantaneous velocity field within the leading-edge vortex is examined. The topology of the velocity vector field at a fixed instant in time may be examined by constructing 3-D streamlines, selected streamsurfaces, as well as, 2-D “sectional streamlines” obtained by the projection of the velocity vector on a given plane (for instance, crossflow plane). Of course, since the flow is unsteady, these instantaneous streamlines do not coincide with actual particle paths and therefore do not provide a true Lagrangian description of the flow field, which remains the subject of future research efforts.

The interpretation of instantaneous 2-D and 3-D streamline patterns is aided considerably by the use of critical-point theory or phase-space analysis originally developed for studying the qualitative behaviour of solutions to ordinary differential equations [36,37]. Critical point theory, as applied to flow patterns, is described extensively in Refs. 23 and 38-41. In the present context, critical (or singular) points are points in the flow where the velocity is zero and the streamline slope is indeterminate. Critical points may be broadly divided into no-slip and free-slip critical points depending upon whether they are located on a no-slip boundary or within the fluid, respectively. For the present study, only the latter type will be considered in describing the vortex breakdown structure above the wing.

The classification of critical points and the elementary flow patterns in their vicinity are obtained by a linearized Taylor-series expansion of the velocity about the critical point [23,40]. In tensor notation, it can be written as $dx_i/d\tau = A_{ij}x_j$ where τ represents a time-like parameter and $A_{ij} = \partial u_i / \partial x_j$ denotes the rate-of-deformation tensor. The local

behavior near the critical point is determined by the eigenvalues and eigenvectors of the Jacobian matrix A_{ij} . The classification of 2-D critical points is shown in Fig. 1a as a function of the trace of A_{ij} (Δ) and the determinant (or Jacobian J) of A_{ij} . The different types of critical points are saddles, and nodes and foci either stable (spiraling in) or unstable (spiraling out) depending upon the sign of Δ .

The general classification of 3-D critical points is given by Chong, Perry and Cantwell [23]. The concept of 3-D critical points has been used [39,40] in the analysis of flows predominantly when the critical points are located on no-slip surfaces or on symmetry planes, and are therefore easily identifiable. In complex flows such as asymmetric vortex breakdown, free-slip critical points cannot be so easily located and in fact, a systematic topological description of this flow is not known to the author. In the present study, the only types of 3-D free-slip critical points encountered in the description of vortex breakdown are spiral/saddles which result when A_{ij} possesses one real and two complex-conjugate eigenvalues. A schematic of an “attracting spiral/saddle” or “stable focus/stretching” is shown in Fig. 1b. As discussed in Ref. 23, the plane defined by the complex eigenvalues contains solution trajectories and the flow spirals around the real eigenvalue direction. A “repelling spiral/saddle” or “unstable focus/compressing” can be obtained from Fig. 1b by simply reversing the sense of the arrows.

Another interesting feature encountered in the topology of sectional streamline patterns is that of “bifurcation lines” or “limit cycles” [40,42]. Figure 1c illustrates a negative closed bifurcation line or stable limit cycle to which other non-closed trajectories asymptote. An unstable limit cycle can be obtained from Fig. 1c by reversing the direction of the arrows. If a limit cycle exists in the sectional streamline pattern, it must enclose at least one critical point which cannot be a saddle. Furthermore, the divergence of the 2-D (projected) velocity field in the plane must change sign in the region where the limit cycle exists [37]. Three-dimensional limit cycles (i.e. isolated closed trajectories in 3-D space to which other trajectories asymptote) are also possible [43], and an example is described later in the instantaneous structure of vortex breakdown.

These basic concepts of critical point theory are helpful in the interpretation of the results to be discussed in the following sections. The topological analysis of the computed flow fields is accomplished using PLOT3D and FAST [44] visualization software. In particular, FAST incorporates a recently developed tool [45] for locating 3-D critical points, as well as a fourth-order Runge-Kutta method with adaptive step-size control for the construction of solution trajectories emanating at these critical points.

3. Results

Calculations were performed for a 75° sweep delta wing at a freestream Mach number of 0.2 and a chord Reynolds number of 9,200. The wing was pitched at a nominal constant non-dimensional pitch rate $\Omega^+ = \Omega C/U_\infty = 0.3$, from an initial angle of attack $\alpha_i = 25^\circ$ to a final angle $\alpha_f = 50^\circ$ (see Fig. 2). The pitch axis was located at the wing trailing edge. The above conditions were selected to allow comparison with the experiments of Magness, Robinson and Rockwell [16] and Lin and Rockwell [19].

3.1 Numerical Resolution Effects

Before proceeding to the discussion of the physical aspects of the flow, results from a limited assessment of the effects of numerical resolution on the computed solution are presented. The sensitivity of the computed flow field to spatial resolution was investigated by employing the two grids described in Section 2.2. The temporal accuracy was checked by computing the flow on one of the grids using two different time steps ($\Delta t^+ = 0.001$ and 0.0005).

The effects of spatial and temporal resolution on the pitching moment coefficient history are shown in Fig. 2. This figure shows that reducing Δt^+ by a factor of 2.0 has essentially no effect on the computed C_m . The pitching moment coefficient histories obtained on the two grids are also in excellent agreement for $t^+ < 2.5$. It should be noted that the pitching moment, on both grids, at $\alpha = 25^\circ$ is -0.081 , which compares well with the experimental value -0.078 reported by Hummel [46] for a 76° sweep delta wing. The effects of numerical resolution on the lift and drag coefficient histories (not included) were found to be even smaller than those for C_m .

The influence of grid resolution and time step on the instantaneous vortex burst location is shown in Fig. 3. Here again, all computations agree reasonably well with each other. Finally, a comparison of the solutions at $t^+ = 2.06$ is provided in Fig. 4 in terms of the axial velocity on a plane normal to the wing and passing through the center of the vortex. The location and extent of the computed reversed-flow regions are seen to be in good agreement. The maximum discrepancy in axial velocity along the core upstream of breakdown between the solutions was 6.0 percent, with higher values obtained on the finer grid.

Although a more systematic numerical resolution study was found to be computationally prohibitive, the previous limited assessment suggests the results are of sufficient quality to merit further analysis. This view is reinforced further by the favorable comparison with experimental measurements which is presented below. The basic evolution and structure of the transient breakdown were found to be the same in all three computations, and only results from the finer grid are discussed in the following sections. This discussion

will be limited to the flow features observed before $t^+ = 2.6$, up to which time sufficient confidence in the calculations exists. Finally, the same sequence of events for transient vortex bursting was also found in computations for different pitch rate and pitch-axis locations to be reported elsewhere [47].

3.2 Evolution of Transient Breakdown

In this section, a description of the initiation and evolution of the breakdown region in the primary leading-edge vortex is provided. In addition to breakdown of the primary vortex, "bursting" or reverse flow in the secondary vortex is also observed. In fact, examination of the computed solution at $t^+ = 0.0$ ($\alpha = 25^\circ$), revealed that breakdown of the secondary vortex occurs prior to the start of the pitching motion. This early breakdown of the secondary vortex, as compared to the main vortex, is consistent with the experimental observations of Lambourne and Bryer [11]. The secondary vortex bursting exerts little influence on the primary flow structure, and therefore details of these secondary features are omitted.

Although the present flow is highly three-dimensional, an overall description of the transient breakdown can be obtained from examination of the flow on a longitudinal plane normal to the wing and passing through the center of the vortex core. The angle between this plane and the wing symmetry plane is approximately 10.3° . Contours of constant axial velocity and selected velocity vector profiles on this plane, as well as the velocity and pressure along the vortex axis¹ are given at various instants in Figs. 5 to 7.

The computed instantaneous position of vortex breakdown, determined from the stagnation point along the vortex axis, is given in Fig. 8, and compared with results from two separate experimental runs by Lin and Rockwell [19]. The computed and experimental vortex breakdown histories are in good overall agreement, and the repeatability in the experiments is noteworthy. As the vortex breakdown moves closer to the apex (say $t^+ > 2.5$), effects of asymmetries in the experiments [16], present for this high wing sweep, preclude a direct comparison with the fully symmetric calculation. Vortex breakdown occurs over the wing only after cessation of the pitching motion ($\alpha = 50^\circ$), and shows a significant lag in relation to the stationary case for which breakdown appears [16] near the trailing edge at $\alpha = 32^\circ$.

Although a precise explanation of the delay and initial location of vortex bursting is not obvious in this highly transient maneuver, several effects are known to play an important role in this process. For instance, at this high pitch rate and with the pitch axis at the

¹For convenience, the vortex axis is defined as a ray emanating from the wing apex and passing through the point of minimum total pressure on a crossflow plane ahead of vortex breakdown

wing trailing edge, the motion induces an apparent longitudinal camber effect [48]. The effective angle of attack at the apex is significantly reduced, and increases along the leading edge in the downstream direction (positive camber). The effective local incidence at the apex and trailing edge differ by approximately 17° . The elimination of vortex bursting over a stationary cambered delta wing has been clearly shown by Lambourne and Bryer [11]. A significant weakening of the leading-edge vortex occurs as a result of the reduction in effective angle of attack. This can be observed by examining the pressure along the vortex axis (Fig. 7). At $t^+ = 1.5$, despite the high angle of attack of 48° , relatively low levels of suction exist in the vortex core near the apex due to the wing pitching motion. In fact, the flow along the vortex core experiences a favorable pressure gradient up to midchord. Shortly afterwards ($t^+ = 1.7$) as the motion ends, and the effective angle of attack increases, high suction levels develop in the vortex core, and an adverse axial pressure gradient appears which promotes breakdown. This severe adverse pressure gradient, imposed abruptly after the end of the pitch maneuver, seems to play a dominant role in the onset of breakdown. This dominant pressure gradient effect was also pointed out by Gursul and Ho [18] for the case of breakdown on delta wings subject to an unsteady freestream.

The pressure gradient along the vortex core becomes more pronounced as breakdown propagates upstream (Fig. 7). As discussed by Hall [6], the pressure gradient along the vortex axis is much higher than that encountered by the flow external to the core. This is apparent in Fig. 7, by comparing the pressure along the axis with the corresponding distribution on the wing surface underneath the vortex, at $t^+ = 2.14$. The maximum magnitude of the adverse axial pressure gradient is a factor of 7.7 larger than the maximum value along the surface. It was also noted in the calculations that the surface pressure does not display significant oscillations due to the transient breakdown until approximately $t^+ = 2.26$, when breakdown is already at $X/C = 0.45$. This may have implications on the early detection of breakdown using surface pressure information.

Another effect of importance in transient breakdown is the convective time lags along the vortex core [11,48]. Subsequent to the cessation of the pitching motion, the axial core velocity near the apex increases (Fig. 6a) as the vortex adjusts to the new higher effective incidence. This adjustment of the vortex propagates downstream with a speed of the order of the freestream velocity. As a result, a transient increase in the adverse axial pressure gradient occurs between the regions of higher and lower axial velocities in the core. This effect can be seen between the points denoted as "A" and "B" in Fig. 7, at $t^+ = 1.8$.

In the highly transient initial stages of breakdown, following deceleration of the wing, two distinct processes take place along the vortex core. Near the apex, the leading-edge vortex adjusts to a higher effective angle of attack, and this "expansion" (i.e. a region of higher axial velocity and lower pressure) propagates downstream. Simultaneously, stagna-

tion of the axial flow occurs near the trailing edge, and the stagnation region propagates upstream. The axial velocity at $t^+ = 1.8$ (Fig. 6a) clearly shows these effects. From point "A" to "B", a rapid reduction in U' exists associated with the lag in the adjustment of the leading-edge vortex. From point "C" to "D", a high deceleration occurs due to the approaching breakdown region. A plateau in the curve exists between these two regions (point "B" to "C"). The extent of this plateau diminishes as the vortex breakdown (moving upstream) and the "vortex expansion" (moving downstream) collide, roughly at $X/C = 0.5$ and $t^+ = 2.1$.

The overall growth and propagation of the breakdown region is shown in Fig. 5. Also discernable in this figure is the increase, near the apex, of the axial velocity in the vortex core. The edge of this region of higher axial velocity moves downstream (Figs 5a-c). At $t^+ = 1.8$ (Fig. 5a), a limited region of axial flow reversal appears ahead of the wing trailing edge, and can be observed to extend rapidly in both the upstream and downstream directions. Details of the vortex breakdown downstream of the wing are not considered due to the diminishing grid resolution in this region. As breakdown penetrates upstream (Figs. 5b,c), the reversed-flow region grows in radial extent, and its nose becomes blunter due to the increase in radial velocity associated with the steepening axial velocity gradient (Fig. 6a). The change in the character of the velocity profiles from a jet-type, upstream of breakdown, to a wake-type, downstream of breakdown, is also apparent in Fig. 5. During this transient breakdown, very high reversed-flow velocity magnitudes are obtained. At $t^+ = 2.3$ (Fig. 6b), this magnitude exceeds twice the freestream velocity, and consequently, a strong shear layer of azimuthal vorticity surrounds the breakdown region.

In the early stages of the process, the breakdown region appears fairly axisymmetric (Figs. 5a,b), however, by $t^+ = 2.26$ (Fig. 5c), some undulations are apparent. These undulations become more pronounced (Figs. 5d,e), and lead eventually (Fig. 5f) to the formation of two distinct regions of negative axial velocity. The forward region seems to correspond to a bubble-type vortex breakdown. It should be noted that on a crossflow plane between these regions, the axial velocity in the core is everywhere positive. As the breakdown undergoes this dramatic transformation, the magnitude of the reversed-flow velocity diminishes significantly (Fig. 6b), and the breakdown rate of propagation also decreases (Fig. 8).

A comparison of the computed reversed-flow region with the experimental data of Lin and Rockwell [19] is given in Fig. 9 at two instants during the unsteady breakdown process. The experimental results clearly display the appearance of the bubble structure predicted in the computation. A comparison of computed and experimental axial velocity profiles at a station through the center of the bubble is also shown in Fig. 10. Given the complexity of this highly unsteady flow, the good agreement in Figs. 9 and 10 is encouraging, and indicates

that the computational approach captures the basic dynamics of the transient breakdown. The emergence of a bubble structure, as the breakdown moves upstream and a stronger transition takes place along the vortex axis (as evidenced, for instance, by the shock-like jump in axial velocity, Fig. 6b), is also consistent with other experimental observations. As shown by Sarpkaya [12] and Faler and Leibovich [13] in their tube experiments, increasing the swirl level leads to the formation of a bubble-type breakdown accompanied by an upstream displacement.

To conclude this section, some brief comments are made on the behavior of the azimuthal vorticity component. The importance of azimuthal vorticity production in the dynamics of vortex breakdown has been recently highlighted by Brown and Lopez [49]. In the case of steady, inviscid, axisymmetric flow, they derive a necessary criterion for the occurrence of breakdown, and discuss the relationship between the production of negative azimuthal vorticity and the radial divergence of the flow. As the axial velocity in the leading-edge vortex evolves from a jet-type to a wake-type profile (Fig. 5), a change in the sign of the azimuthal vorticity component takes place. This is shown in Fig. 11a at $t^+ = 2.26$ on a vertical plane through the vortex core. The reversed-flow region is contained within the larger domain of negative azimuthal vorticity, and the switch in the vorticity sign occurs upstream of the stagnation point. It should be noted that these observations are also in qualitative agreement with the experiments of Towfighi and Rockwell [20] and Lin and Rockwell [19]. An instantaneous vortex line passing approximately through the center of the vortex core upstream of breakdown is shown in Fig. 11b. Downstream of the stagnation point, the vortex line spirals in a sense opposite to that of the base flow, which is of course consistent with the switch in sign of the azimuthal vorticity component. Details of the evolution and dynamics of the vorticity field during the transient breakdown will be presented in Ref. 50.

3.3 Topology of Sectional Streamlines

The instantaneous crossflow topology on a pitching delta wing has been investigated experimentally by Magness, Robinson and Rockwell [16]. In their study, it was found for the first time that in the aft region above the wing just ahead of breakdown, the topology associated with the leading edge vortex is characterized by an unstable focus. This result is in contrast with the usually assumed crossflow topology consisting of a stable focus. As noted in Ref. 16, the variation of the crossflow topology along the chord of the wing could not be fully determined, and questions regarding the transformation from a stable to an unstable pattern could not be resolved. The present computational results can be used to confirm and extend the previous experimental findings.

The evolution of the computed crossflow topology along the wing is shown in Fig. 12 at $t^+ = 2.06$, when breakdown is at $X/C = 0.6$. Near the apex ($X/C = 0.13$), the topology of the primary vortex is characterized by the usually assumed stable focus (Fig. 12a). At $X/C = 0.34$ (Fig. 12b), the sectional streamlines emanating from the leading edge spiral inward but the streamlines in the core are seen to spiral outward. As a result, a stable limit cycle (Fig. 1c) exists between the two regions. At the location $X/C = 0.6$ (Fig. 12c), the topology is characterized by an unstable focus as previously found by Magness et al. [16]. Finally, at $X/C = 0.9$ (Fig. 12d), downstream of breakdown, the flow in the core begins to spiral inward while away from the axis the flow spirals outward, and an unstable limit cycle appears. The calculations reveal that the transformation of the crossflow topology from a stable to an unstable focus (or vice versa) takes place through the appearance of closed bifurcation lines or limit cycles. One should note that limit cycles in sectional streamline patterns have been previously observed on a plane which cuts a multi-celled vortical structure [40]. However, the limit cycle of Fig. 12b, which occurs well upstream of vortex breakdown, is not associated with such multiple cells or reverse flow in the vortex, but rather with the axial deceleration and radial divergence of the flow.

The type of 2-D critical point in the crossflow pattern (i.e. where $v = w = 0$) associated with the vortex axis is determined (see Fig. 1a) by the divergence $\Delta = v_Y + w_Z$ and the Jacobian $J = v_Y w_Z - v_Z w_Y$ of the projected velocity field. If $J > \Delta^2/4$, the critical point is a focus, either stable for $\Delta < 0$, or unstable for $\Delta > 0$. For the pattern of Fig. 12b, $J/(U_\infty C)^2 = 2.5 \times 10^4$ and $\Delta/(U_\infty C) = 4.5$ and therefore the focus must be unstable. Since the outer flow is spiraling inward, a limit cycle then appears, and contains a region with both positive and negative values of Δ . If the flow is assumed to be effectively incompressible, Δ can be approximated by $-\partial u / \partial X$ using the equation of mass conservation. In fact, the patterns of Fig. 12 may be correlated with the corresponding axial velocity distribution along the core given in Fig. 6a. For $X/C = 0.13$ and 0.9 (Figs. 12a,d), the axial velocity gradient is positive (vortex stretching) and the sectional streamlines possess a stable focus. On the other hand, for $X/C = 0.34$ and 0.6 , an unstable focus is present due to the negative axial velocity gradient (vortex compression). Since sectional streamline patterns are not necessarily invariant with the orientation of the plane [39,42], the crossflow topology was re-examined on transverse planes normal to the vortex axis, but was found to be essentially the same. Therefore, the various topologies of Fig. 12 are not due to the angle of the plane relative to the vortex axis (as could be the case [42]), but rather to stretching and compression of the vortex core.

The previous straightforward application of critical point theory to the interpretation of sectional streamline patterns also suggests that the various crossflow topologies observed are not restricted to the case of vortex breakdown. For instance, even for steady vortical

flow past a stationary wing [34], the crossflow topology (at $X/C = 0.6$) is found to be characterized by an unstable focus and limit cycle, and not by the usual stable focus. The standard interpretation found in the literature for the crossflow topology of vortical flows past delta wings and forebodies is clearly not universally valid.

Although the previous discussion has been restricted to the primary vortex, different crossflow topologies are also possible for the secondary vortical structures (see Figs. 12b,d and Ref. 34). Furthermore, unstable foci and limit cycles are also found (but not included here) in the topology of the vorticity vector field projected on a transverse plane.

The evolution of the sectional streamlines on the longitudinal plane through the vortex core was also examined. The topology on this plane, unlike that for a crossflow plane, displayed sensitivity to the orientation of the plane itself. Therefore, only the pattern corresponding to the breakdown bubble of Fig. 5f is discussed since it was found to persist at various instants in time. The computed bubble topology is shown in Fig. 13, and is compared with the experimental results of Lin and Rockwell [19]. The computed and experimental patterns in the breakdown bubble have equivalent topologies since they display the same number, type and connectivity of critical points. This pattern, sketched for clarity in Fig. 13d, is characterized by two saddles (S_1, S_2), a stable focus (F^+) and an unstable focus (F^-), and displays no saddle-saddle connections. In the calculations it was found that the 3-D bubble (to be described in the next section) rotates about the vortex axis in the same sense as the base flow. As a result, the sectional streamline pattern undergoes structural bifurcations [39,41], although the basic 3-D structure remains unchanged in a frame of reference rotating with it. In Figs. 13b,c, the foci switch position relative to the wing as the bubble rotates. The instantaneous sectional topology indicates that the bubble is open, thereby allowing upstream flow to go into the bubble, as well as, flow from inside the bubble to exit downstream. The computational and experimental instantaneous bubble structure of Fig. 13 differs from the mean axisymmetric topologies described by Falor and Leibovich [14] and Bornstein and Escudier[15]. However, the relationship between the instantaneous and mean representations of the breakdown bubble requires further investigation.

3.4 Three-Dimensional Topology of Vortex Breakdown

Although sectional streamlines can provide information on the structure of a complex three-dimensional flow, interpretation based solely on them is incomplete when there is a component of velocity out of the plane under consideration. One should also note that the 2-D critical points on a planar portrait are not necessarily associated with true critical points of

the three-dimensional vector field. In order to systematically describe the complex instantaneous structure of breakdown above the wing, the three-dimensional velocity vector field is examined, and its topology is characterized in terms of the associated 3-D critical points. The 3-D free-slip critical points in the breakdown region are shown in Figs. 14-17, along with selected streamlines emanating from or reaching the critical points. For the purpose of reference, the iso-surface of zero axial velocity is also included in Fig. 16.

At $t^+ = 1.8$ (Fig. 14), two critical points or stagnation points are observed at the beginning and end of the breakdown region. Point S_1^- is a repelling spiral/saddle, while S_1^+ is an attracting spiral/saddle (see Section 2.3 and Fig. 1b). Only streamlines reaching (red) and leaving (yellow) S_1^+ are shown in Fig. 14a. Similarly, trajectories approaching (green) and leaving (white) S_1^- are included in Fig. 14b. At its onset, the vortex breakdown region, defined by these critical points and associated trajectories, is fairly axisymmetric. As the region of reverse flow grows, point S_1^+ moves downstream of the wing trailing edge and out of the chosen domain of observation, whereas S_1^- proceeds upstream. Later in time ($t^+ = 2.06$, Fig. 15), therefore only one critical point (S_1^-) is seen, and corresponds to the main stagnation point associated with vortex breakdown. Within the reversed-flow region, the streamlines spiral upstream toward S_1^- .

By $t^+ = 2.26$ (Fig. 16a), an additional pair of spiral/saddle critical points, denoted as S_2^+ (attracting) and S_2^- (repelling) have emerged. At the instant of the picture, the stagnation points (S_2^+, S_2^-) are located at approximately the same radial distance from the vortex axis on the iso-surface of zero axial velocity and are separated by an azimuthal angle of 85° . These additional critical points show that multiple stagnation points may exist in the breakdown region. A closer look at the way in which S_2^+ and S_2^- are connected (Fig. 16b) reveals an interesting structure. The streamsurface associated with the trajectories spiraling toward S_2^+ wraps around a closed loop in 3-D space, as shown schematically in Fig. 16c. This closed trajectory is a repelling limit cycle, the three-dimensional extension of the (2-D) limit cycles previously described in reference to the sectional streamline patterns. A better pictorial representation of this type of vector field feature can be found in Ref. 43.

Observation of the 3-D velocity field at various instants in time shows that the critical points (S_2^+, S_2^-) rotate in the same sense as the base flow, and move apart from each other in the azimuthal direction. By $t^+ = 2.34$, the approximate azimuthal angle between S_2^+ and S_2^- is 160 degrees. Although the reason for the appearance of these critical points is not yet known, they suggest the existence of a growing non-axisymmetric or azimuthal disturbance. As discussed by Leibovich [8], as the main axisymmetric wave reaches a critical amplitude, instability of the flow to three-dimensional disturbances and transfer of energy to non-axisymmetric modes occur. The possible relationship between these rotating stagnation

points and the experimentally observed coherent oscillations in vortex breakdown requires further elucidation.

As previously discussed in reference to Fig. 5f, by $t^+ = 2.4$, the breakdown has evolved into two distinct regions of reverse flow. The corresponding 3-D topology, given in Fig. 17, indicates the appearance of an additional pair of critical points (S_3^+ , S_3^-). Point S_3^+ is an attracting spiral/saddle associated with the closing of the bubble while point S_3^- , similar to S_1^- , is a repelling spiral/saddle located at the nose of the aft breakdown region. Although only three instantaneous streamlines (corresponding to the three eigenvector directions) are shown for each critical point, the complexity of the flow is quite apparent. In Fig. 17a, only the trajectories reaching (red) and leaving (yellow) the attracting spiral/saddles are shown. Similarly, the streamlines approaching (green) and leaving (blue) the repelling critical points (S_1^-, S_2^-, S_3^-) are included in Fig. 17b. The spiraling trajectory reaching S_2^+ (denoted as "1" in Fig. 17a) goes into the bubble, and confirms that the bubble structure is open. Similarly, the trajectory emanating from S_2^- (denoted as "2" in Fig. 17b) goes out of the bubble and spirals along the vortex axis downstream of the bubble. It should also be noted that S_2^+ and S_2^- are approximately 170° apart in azimuth. The above bubble characteristics correlate with the experiments of Sarpkaya [12] and Faler and Leibovich [13] who report open breakdown bubbles which are filled and emptied at diametrically opposed points.

The relation between the present instantaneous (streamline) structure of breakdown and the available experimental flow visualizations (streaklines) is by no means clear. The complexity revealed by the instantaneous velocity field indicates, however, that that interpretation of the flow structure based solely on standard visualizations is not fully satisfactory. Attempts to generate a streakline representation of the computed transient breakdown for the purpose of comparison were not very successful. Although this is in principle straightforward, the final appearance of the computed streaklines was found to be highly dependent on the initial distribution of the "seeded particles". Since the core of the vortex is a region of low total pressure, an alternative representation of breakdown was sought using this scalar quantity. Figure 18a shows an iso-surface of constant total pressure at $t^+ = 2.4$. One can clearly observe the vortex core upstream of stagnation, its swelling and bubble formation, as well as a "tail" which spirals in the opposite sense of the basic flow (indicated by the yellow streamline). The computed structure is quite similar to the experimental flow visualization of "axisymmetric" breakdown in a tube obtained by Faler and Leibovich [13], which is reproduced for convenience in Fig. 18b. This resemblance indicates that vortex bursting over a delta wing at high angle of attack is more closely related to vortex breakdown in a tube than previously thought.

4. Conclusions

Computational results have been presented which describe the initiation and evolution of transient vortex breakdown above a delta wing subject to a pitch-and-hold maneuver. The assessment of the effects of numerical resolution, and the favorable comparison with available experimental data suggest that the computational approach captures the basic dynamics of this transient breakdown.

The angular delay and onset of breakdown are strongly linked to the pressure gradient prevailing along the vortex axis. This pressure gradient, which depends on the wing angle of attack and pitching motion, plays a dominant role in the initiation of vortex breakdown.

A description of the 3-D instantaneous structure of vortex breakdown is provided for the first time using critical-point theory. The region of reverse flow in the vortex core is associated with the appearance of pairs of opposite 3-D spiral/saddle critical points. During its early stages, the vortex breakdown is fairly axisymmetric. However, as it proceeds upstream, and a stronger transition takes place along the axis, asymmetric effects become increasingly important and lead eventually to the formation of a breakdown bubble. This bubble structure is open and contains within itself a pair of stagnation points which are diametrically opposed and which rotate in the same sense as the base flow. These critical points suggest the existence of azimuthal disturbances, and their rotation might be linked with the coherent oscillations observed in vortex breakdown.

A representation of the breakdown bubble using an iso-surface of constant total pressure shows a great deal of resemblance to experimental flow visualizations of axisymmetric vortex breakdown in a tube. Further investigation of the relation between the different representations of the breakdown region (i.e. instantaneous flow structure, streakline visualizations and mean-flow measurements) should be pursued, preferably for unsteady breakdown above a stationary delta wing. Knowledge of the 3-D structure will provide guidance for the development of a comprehensive theory of vortex breakdown which is still lacking.

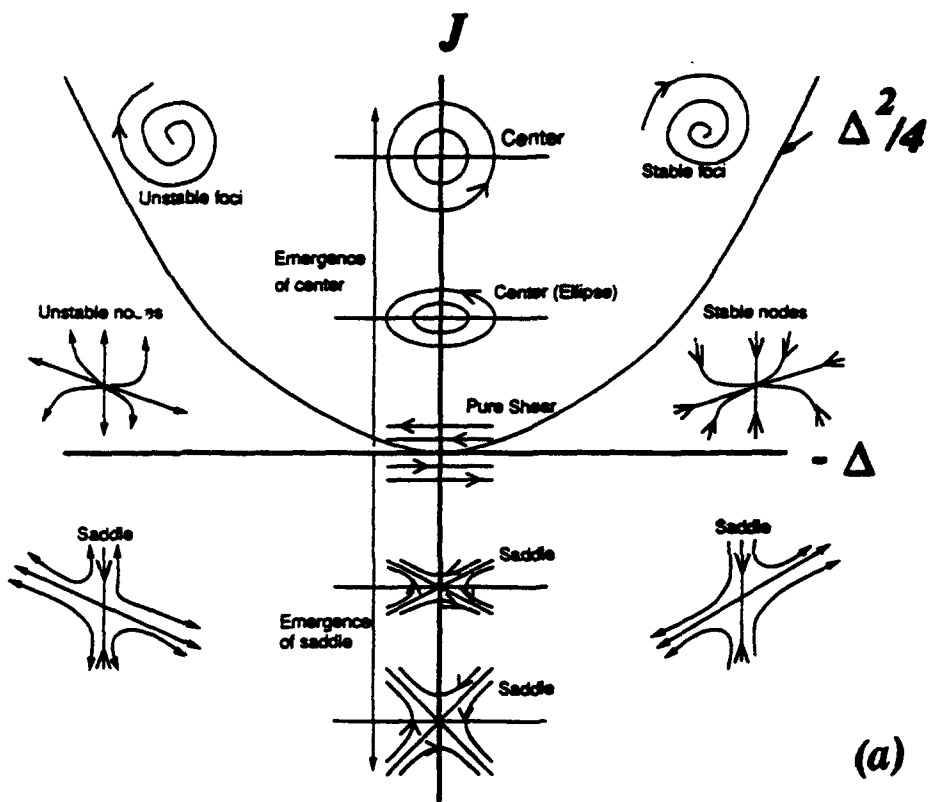
5. References

1. Ashley H., Katz, J., Jarrah, M-A and Vaneck, T., "Unsteady Aerodynamic Loading of Delta Wings for Low and High Angles of Attack," in International Symposium on Nonsteady Fluid Dynamics (Eds. Miller, J. and Telionis D.), ASME Fluids Engineering Division Vol. 92, 1990.
2. Magness, C, Robinson, O. and Rockwell, D., "Control of Leading-Edge Vortices on a Delta Wing," AIAA Paper 89-0999, 1989.
3. Jarrah, M-A., "Low-Speed Wind-Tunnel Investigation of Flow About Delta Wings, Oscillating in Pitch to Very High Angle of Attack," AIAA Paper 89-0295, January 1989.
4. Reynolds, G. and Abtahi, A., "Instabilities in Leading-Edge Vortex Development," AIAA Paper 87-2424, 1987.
5. Bragg, M. B. and Soltani, M. R., "Measured Forces and Moments on a Delta Wing During Pitch-Up," J. Aircraft, Vol. 27, No.3, March 1990.
6. Hall, M. G., "Vortex Breakdown," Ann. Rev. Fluid Mech., 4, 1972.
7. Leibovich, S., "The Structure of Vortex Breakdown", Ann. Rev. Fluid Mech., 10, 1978.
8. Leibovich, S., "Vortex Stability and Breakdown: Survey and Extension," AIAA J., Vol. 22, No. 9, pp. 1192-1206, September 1984.
9. Escudier, M., "Vortex Breakdown: Observations and Explanations," Prog. Aerospace Sci., Vol. 25, pp. 189-229, 1988.
10. Leibovich, S. and Kribus, A., "Large-Amplitude Wavetrains and Solitary Waves in Vortices," JFM, Vol. 216, pp. 459-504, 1990.
11. Lambourne, N. C. and Bryer, D. W., "The Bursting of Leading- Edge Vortices- Some Observations and Discussion of the Phenomenon," Reports and Memoranda No. 3282, April 1961.
12. Sarpkaya, T., "On Stationary and Travelling Vortex Breakdowns," JFM, Vol. 45, Part 3, pp. 545-559, 1971.
13. Faler, J. and Leibovich, S., "Disrupted States of Vortex Flow and Vortex Breakdown," Phys. Fluids, Vol. 20, No. 9, September 1977.
14. Faler, J. and Leibovich, S., "An Experimental Map of the Internal Structure of a Vortex Breakdown," JFM, Vol. 86, Part 2, pp. 313-335, 1978.
15. Bornstein, J. and Escudier, M., "LDA Measurements within a Vortex-Breakdown Bubble," Laser Anemometry in Fluid Mechanics, Ladoan-Instituto Superior Tecnico, 1984.
16. Magness, C., Robinson, O. and Rockwell, D., "Instantaneous Topology of the Unsteady Leading-Edge Vortex at High Angle of Attack," AIAA J. (in press).
17. Rediniotis, O., Klute, S., Hoang, N. and Telionis D., "Pitching-Up Motions of Delta Wings," AIAA Paper 92-0278, January 1992.

18. Gursul, I. and Ho, C-M, "Vortex Breakdown Over Delta Wings in Unsteady Free Stream," AIAA Paper 93-0555, January 1993.
19. Lin, J.-C. and Rockwell, D., "Transient Structure of Vortex Breakdown on a Delta Wing at High Angle of Attack," manuscript in preparation, 1992.
20. Towfighi, J. and Rockwell, D., "Instantaneous Structure of Vortex Breakdown on a Delta Wing via Particle Image Velocimetry," AIAA J. (in press).
21. Spall, R., Gatski, T. and Ash, R., "The Structure and Dynamics of Bubble-Type Vortex Breakdown," Proc. R. Soc. Lond. A, 429, pp. 613-637, 1990.
22. Krause, E., "The Solution to the Problem of Vortex Breakdown," Lecture Notes in Physics, 371, K. W. Morton (Ed), 1990.
23. Chong, M. S., Perry, A. E. and Cantwell, B. J., "A General Classification of Three-Dimensional Flow Fields," Physics of Fluids A, Vol. 2, 1990.
24. Pulliam, T.H. and Steger, J.L., "Implicit Finite-Difference Simulation of Three-Dimensional Compressible Flow," AIAA J., Vol. 18, No. 2, February 1980.
25. Beam, R.M. and Warming, R.F., "An Implicit Factored Scheme for the Compressible Navier-Stokes Equations," AIAA J., Vol. 16, No. 4, April 1978.
26. Pulliam, T., "Artificial Dissipation Models for the Euler Equations," AIAA J., Vol. 24, No. 12, pp. 1931-1940, December 1986.
27. Rai, M. and Chakravarthy, S., "An Implicit Form of the Osher Upwind Scheme," AIAA J., Vol. 24, No. 5, pp. 735-743, May 1986.
28. Gordnier, R. E. and Visbal M. R., "Numerical Simulation of the Unsteady Flow Structure over a Delta Wing," AIAA Paper 91-1811, June 1991, (to appear in J. of Aircraft).
29. Visbal, M. and Shang, J., "Investigation of the Flow Structure Around a Rapidly Pitching Airfoil," AIAA J., Vol. 27, No. 8, pp. 1044-1051, August 1989.
30. Visbal, M. R., "Numerical Investigation of Laminar Juncture Flows," AIAA Paper 89-1873, June 1989.
31. Webster, W. P. and Shang, J. S., "Comparison Between Thin- Layer and Full Navier-Stokes Simulations Over a Supersonic Delta Wing," AIAA J., Vol. 29, No. 9, pp. 1363-1369, September 1991.
32. Visbal, M., "Structure of Laminar Juncture Flows," AIAA J., Vol. 29, No. 8, pp. 1273-1282, August 1991.
33. Stanek, M. and Visbal, M., "Investigation of Vortex Development on a Pitching Slender Body of Revolution," AIAA Paper 91-3273, September 1991, (to appear in J. of Aircraft).
34. Gordnier, R. and Visbal, M., "Numerical Simulation of Delta-Wing Roll," AIAA Paper 93-0554, January 1993.
35. Whitfield, D., "Three-Dimensional Unsteady Euler Equation Solutions using a Flux Vector Splitting," Short Course on Numerical Grid Generation, Mississippi State University,

June 1984.

36. Boyce, W. and DiPrima, R., *Elementary Differential Equations and Boundary Value Problems*, 3rd Ed., John Wiley and Sons, 1977.
37. Arrowsmith, D. and Place, C., *Ordinary Differential Equations*, Chapman and Hall Mathematical Series, London, 1982.
38. Tobak, M. and Peake, D., "Topology of 3D Separated Flows," *Ann. Rev. Fluid Mech.*, 14, 61-85, 1982.
39. Chapman, G. T. and Yates, L. A., "Topology of Flow Separation on Three-Dimensional Bodies," *Applied Mechanics Reviews*, Vol. 44, No. 7, July 1991.
40. Perry, A. and Chong, M., "A Description of Eddying Motions and Flow Patterns using Critical-Point Concepts," *Ann. Rev. Fluid Mech.*, 19, pp. 125-155, 1987.
41. Dallmann, U., "On the Formation of Three-Dimensional Vortex Flow Structures," DFVLR Report IB 221-85 A 13, DFVLR-AVA, Gottingen, 1985.
42. Perry, A. and Steiner, T., "Large-Scale Vortex Structures in Turbulent Wakes Behind Bluff Bodies. Part 1. Vortex Formation," *JFM*, Vol. 174, pp. 233-270, 1987.
43. Abraham, R. and Shaw, C., *Dynamics- The Geometry of Behavior, Part 2 : Chaotic Behavior*, Aerial Press, 1982.
44. Bancroft, G., Merritt, F., Plessel, T., Kelaita, P., McCabe, R. and Globus, A., "FAST: A Multi-Processing Environment for Visualization of CFD," *Proc. Visualization '90*, IEEE Computer Society, 1990.
45. Globus, A., Levit, C. and Lasinski, T., "A Tool for Visualizing the Topology of Three-Dimensional Vector Fields," *Visualization '91*, 1991.
46. Hummel, D., "On the Vortex Formation over a Slender Wing at Large Angles of Incidence," AGARD CP-247, 1979.
47. Visbal, M. and Gordnier, R., "Parametric Effects on Vortex Breakdown above a Delta wing," manuscript in preparation, 1993.
48. Ericsson, L. E. and Reding, J. P., "Fluid Dynamics of Unsteady Separated Flow. Part II. Lifting Surfaces," *Prog. Aerospace Sci.*, Vol. 24, pp. 249-356, 1987.
49. Brown, G. and Lopez, J. , "Axisymmetric Vortex Breakdown, Part 2. Physical Mechanisms," *JFM*, Vol. 221, pp. 553-576, 1990.
50. Visbal, M., "Computational Study of Vortex Breakdown on a Pitching Delta Wing," manuscript in preparation, 1993.



(a)

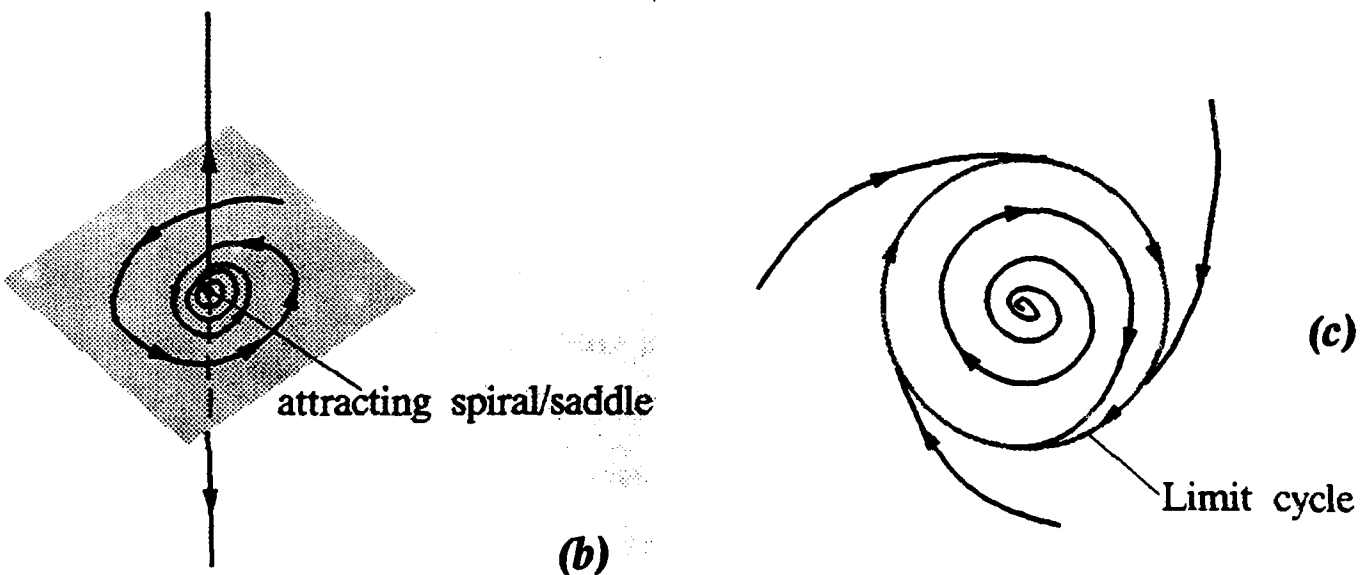


Figure 1: Critical-Point Concepts

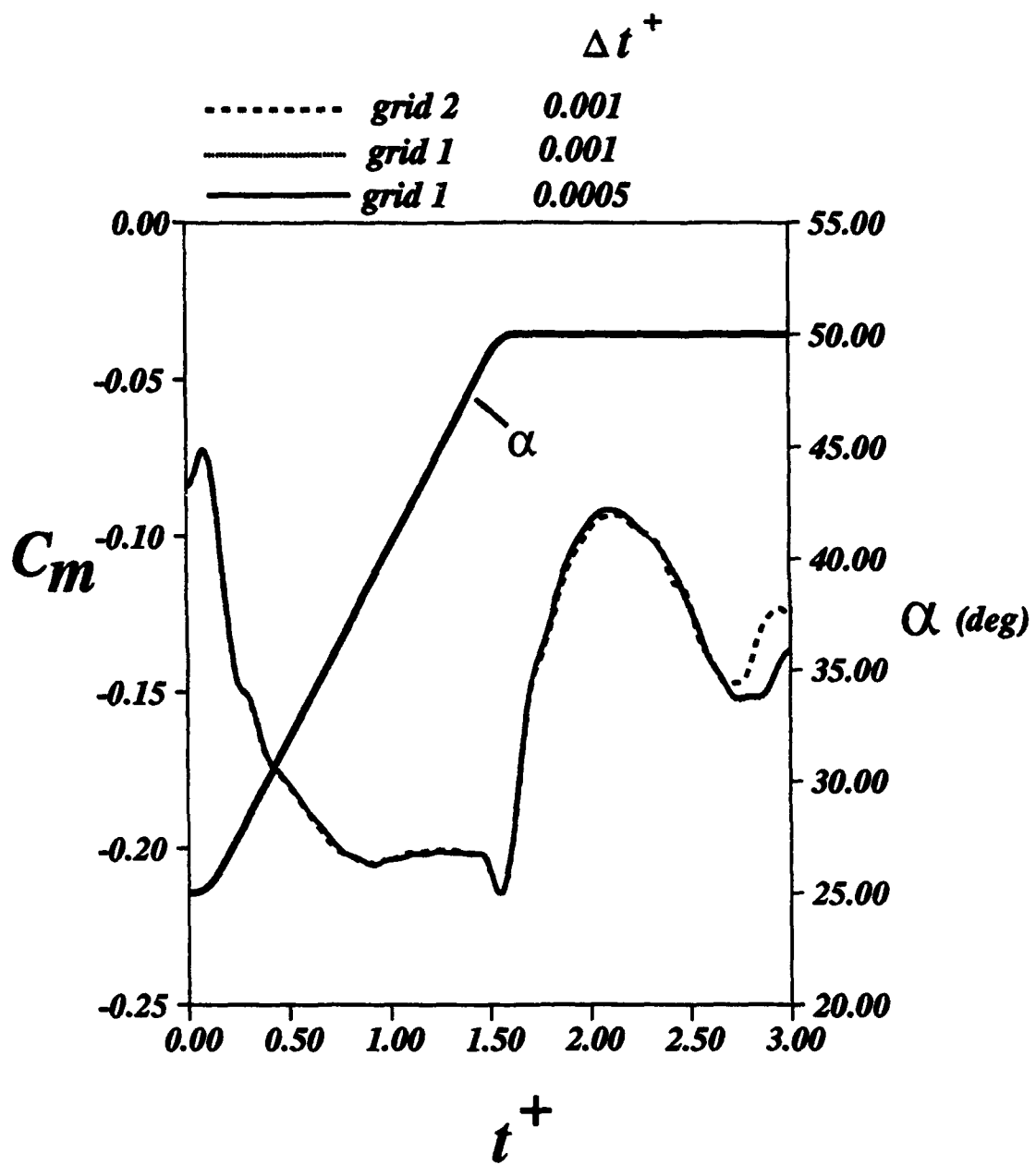


Figure 2: Effect of Numerical Resolution on Computed Pitching Moment Coefficient

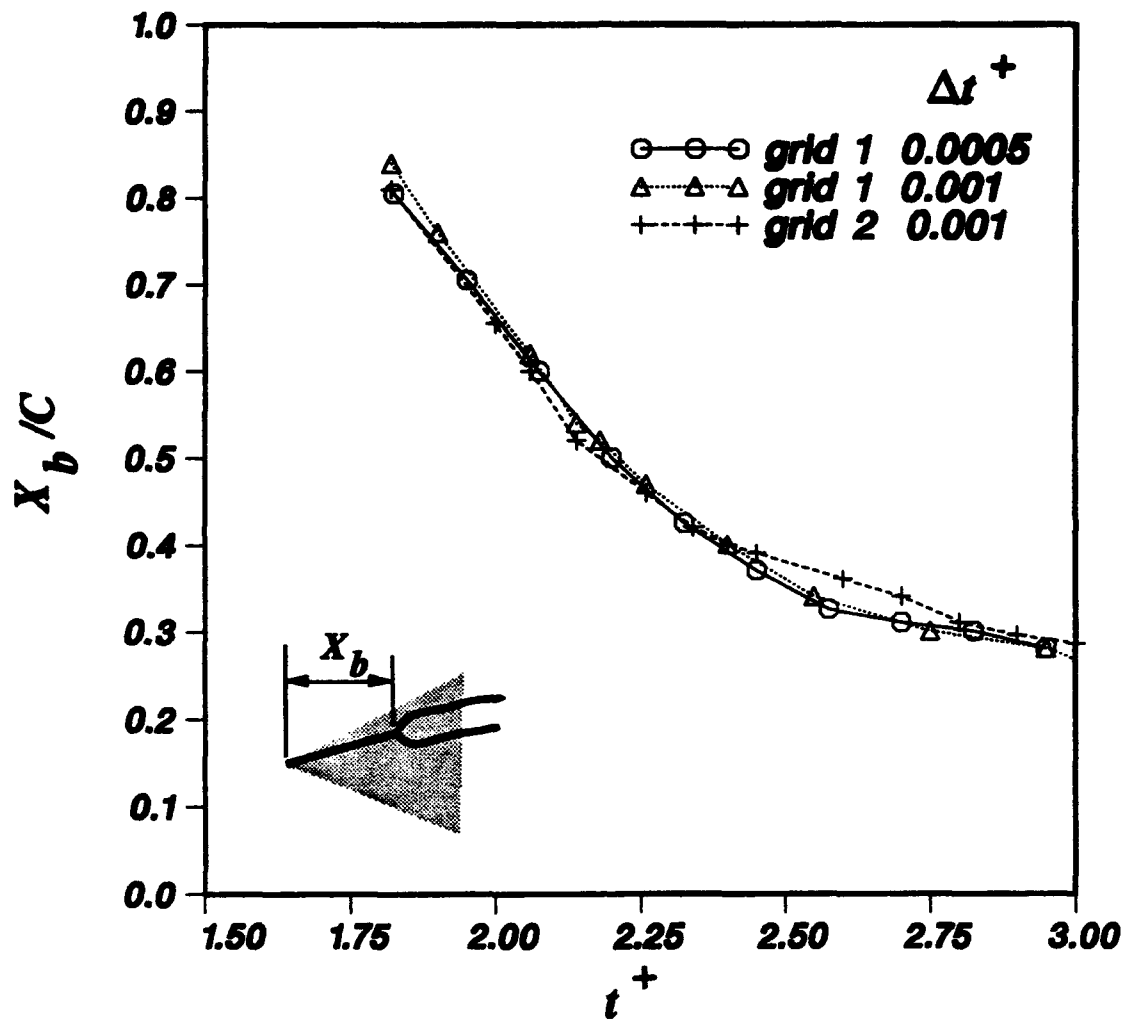


Figure 3: Effect of Numerical Resolution on Vortex Burst Location

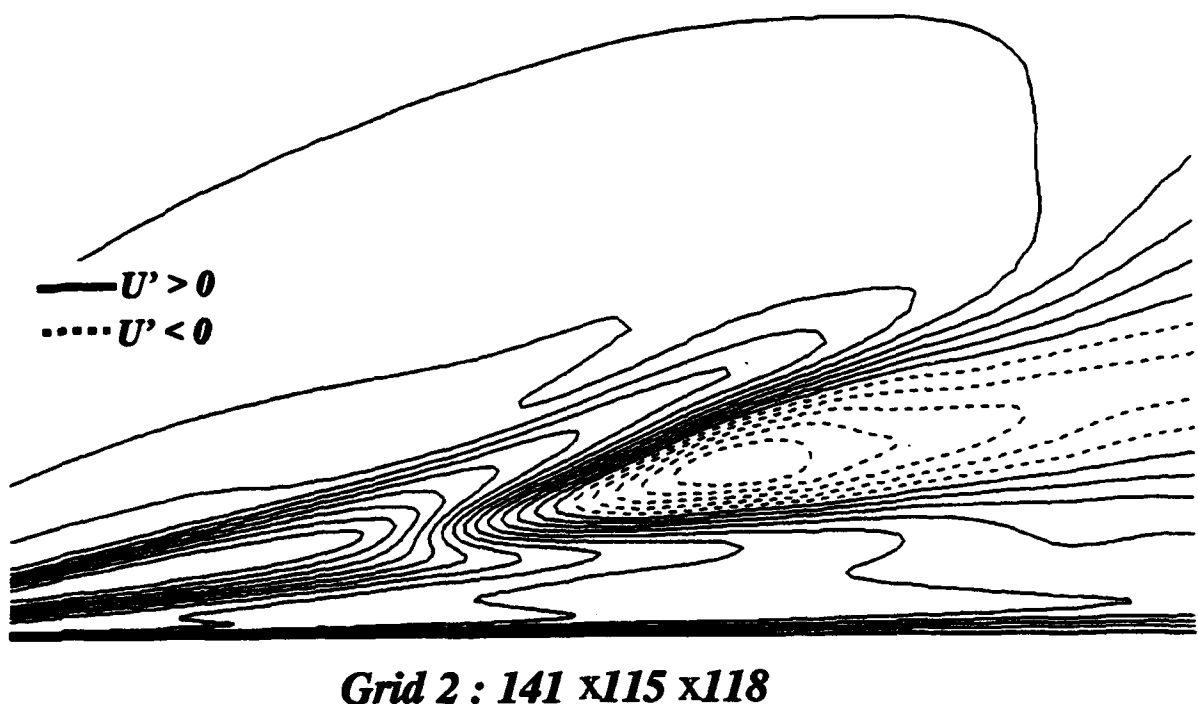
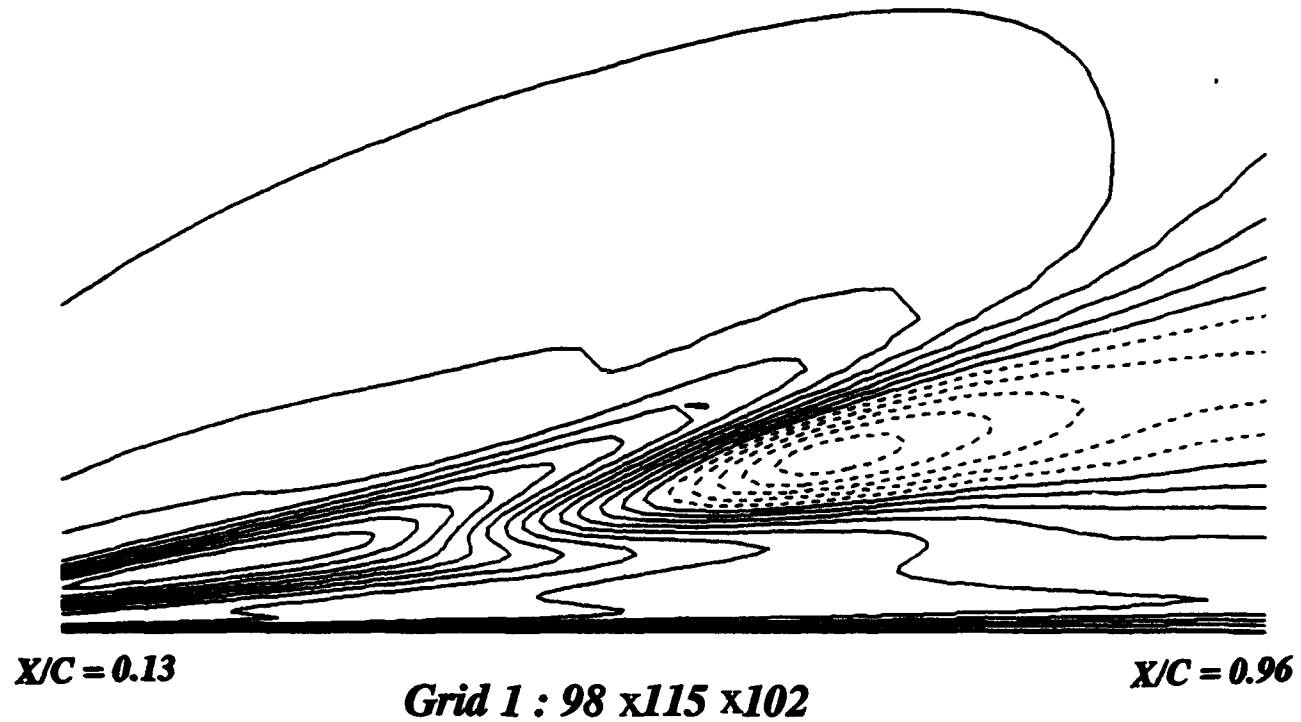


Figure 4: Effect of Grid Resolution on Axial Velocity in a Vertical Plane Through Vortex Core at $t^+ = 2.14$. (Contours of U'/U_∞ from -3.0 to 3.0 in 0.2 increments)

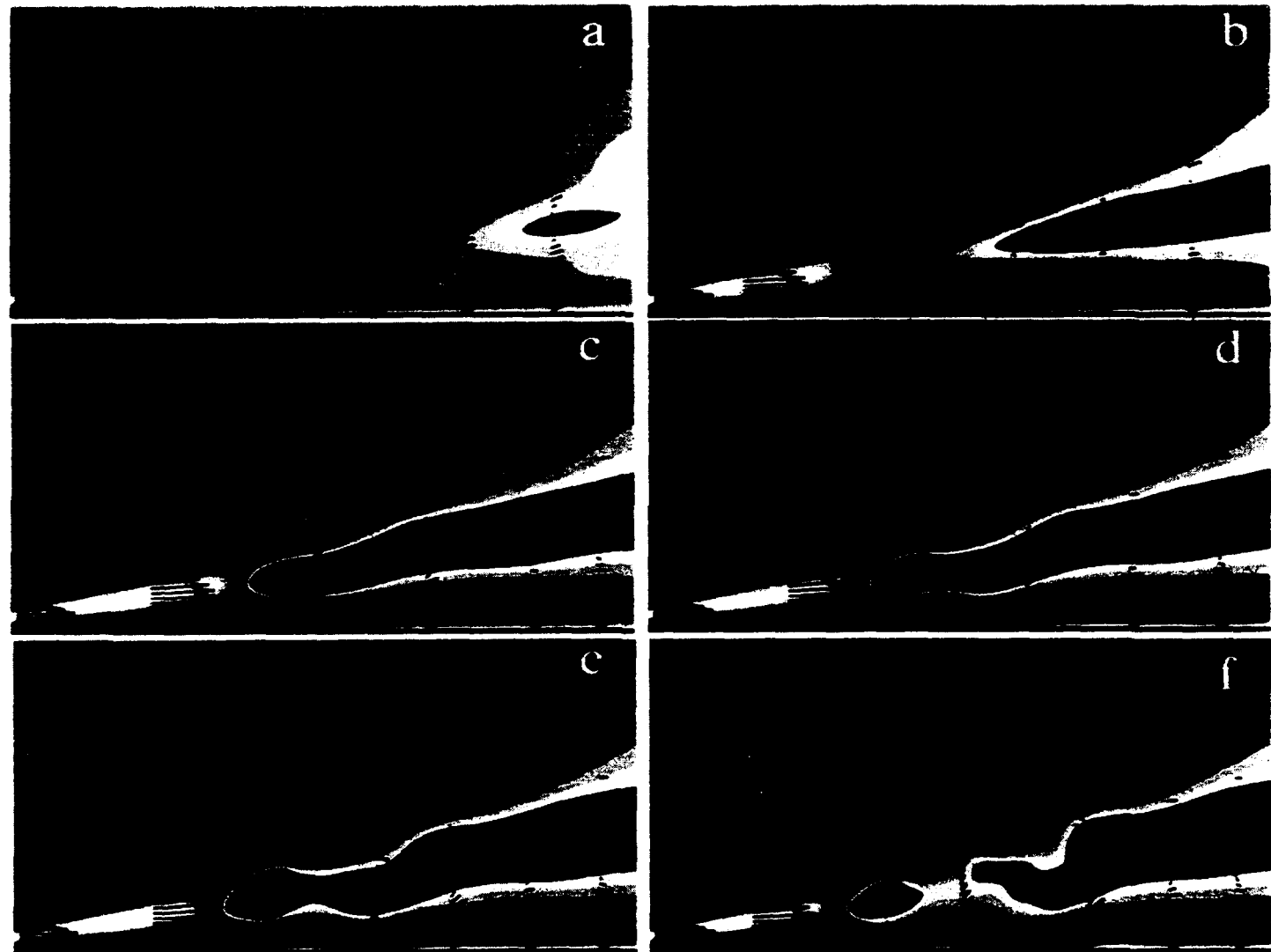


Figure 5: Axial Velocity Contours and Velocity Vectors on Plane Through Vortex Core at $t^+ = 1.8, 2.06, 2.26, 2.3, 2.34$ and 2.4

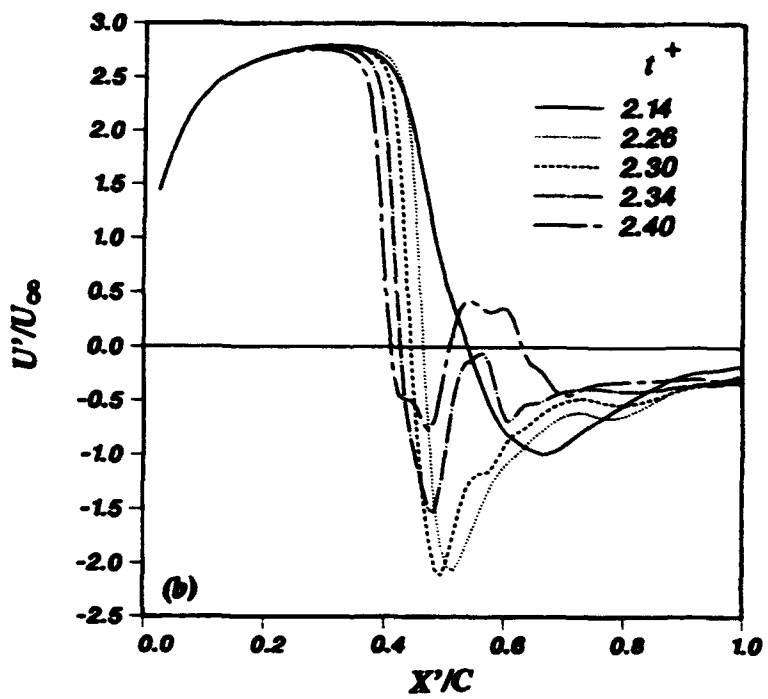
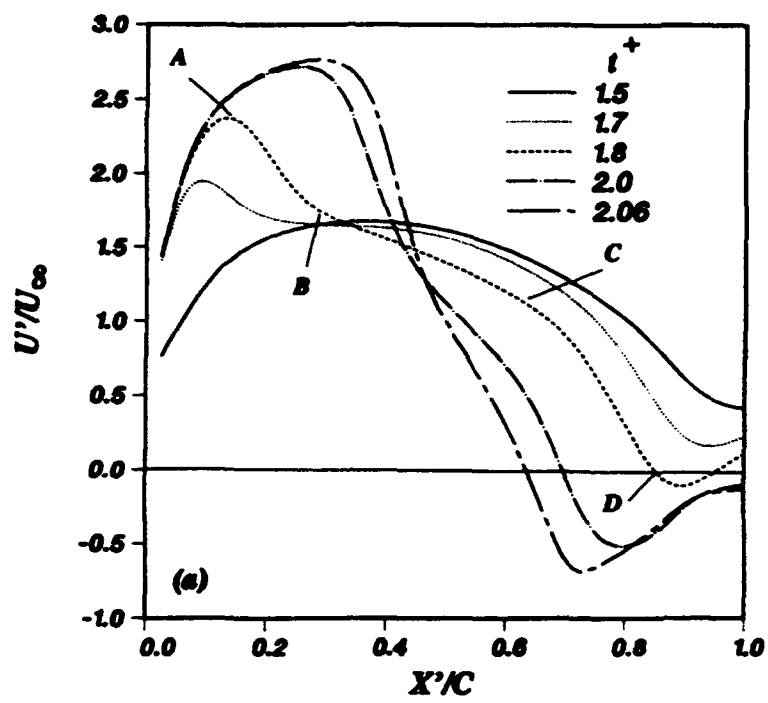


Figure 6: Evolution of Axial Velocity Component along Vortex Axis During Transient Breakdown

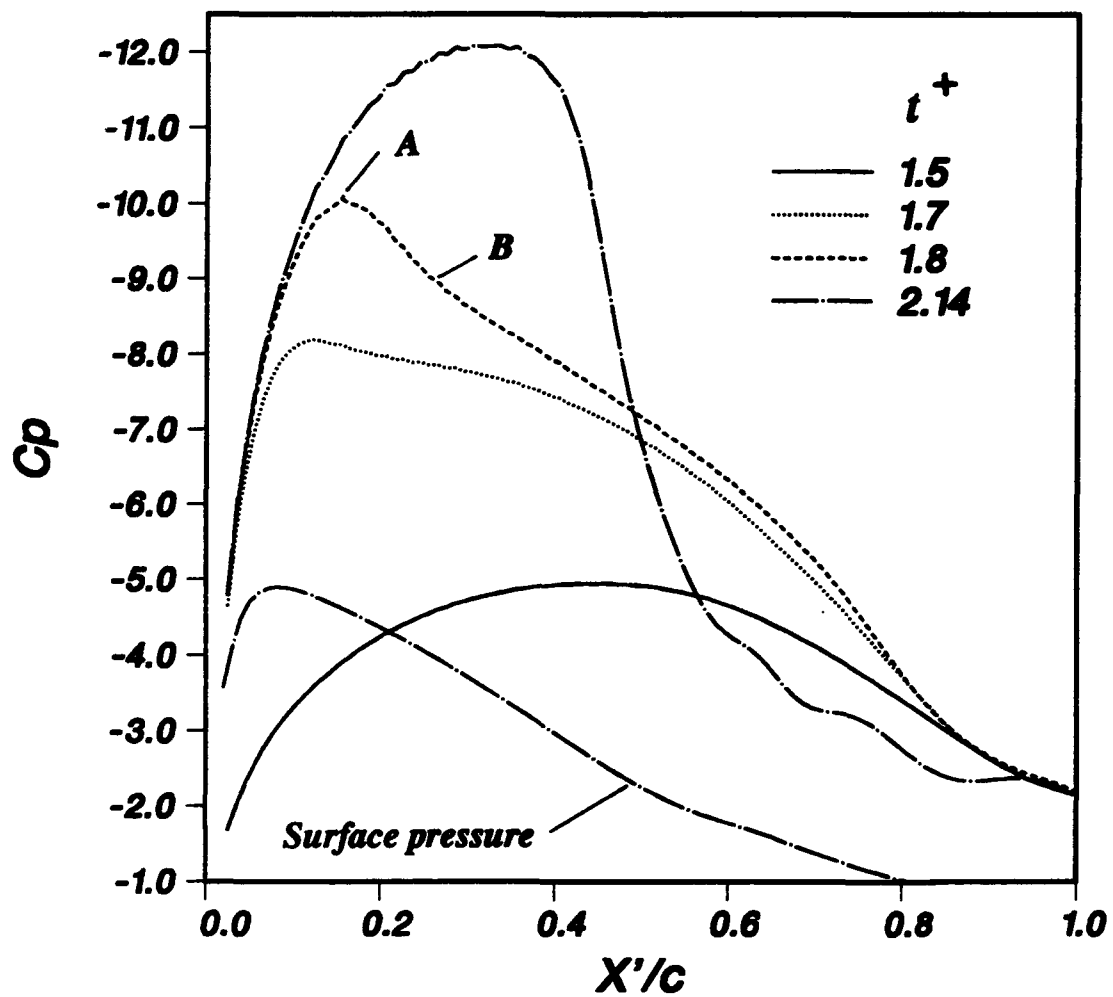


Figure 7: Evolution of Pressure Along Vortex Axis During Transient Breakdown

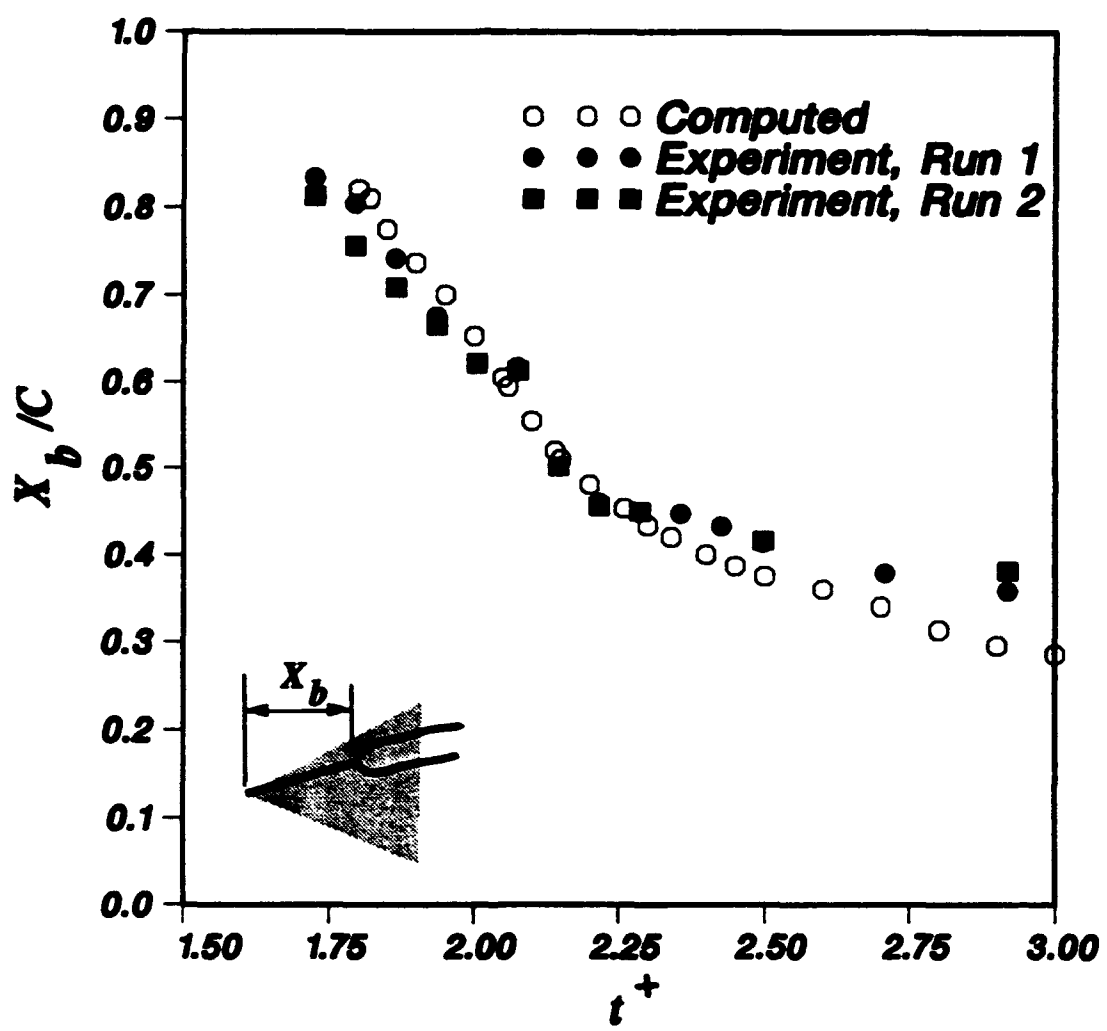


Figure 8: Comparison of Computed and Experimental [19] Vortex Breakdown Locations

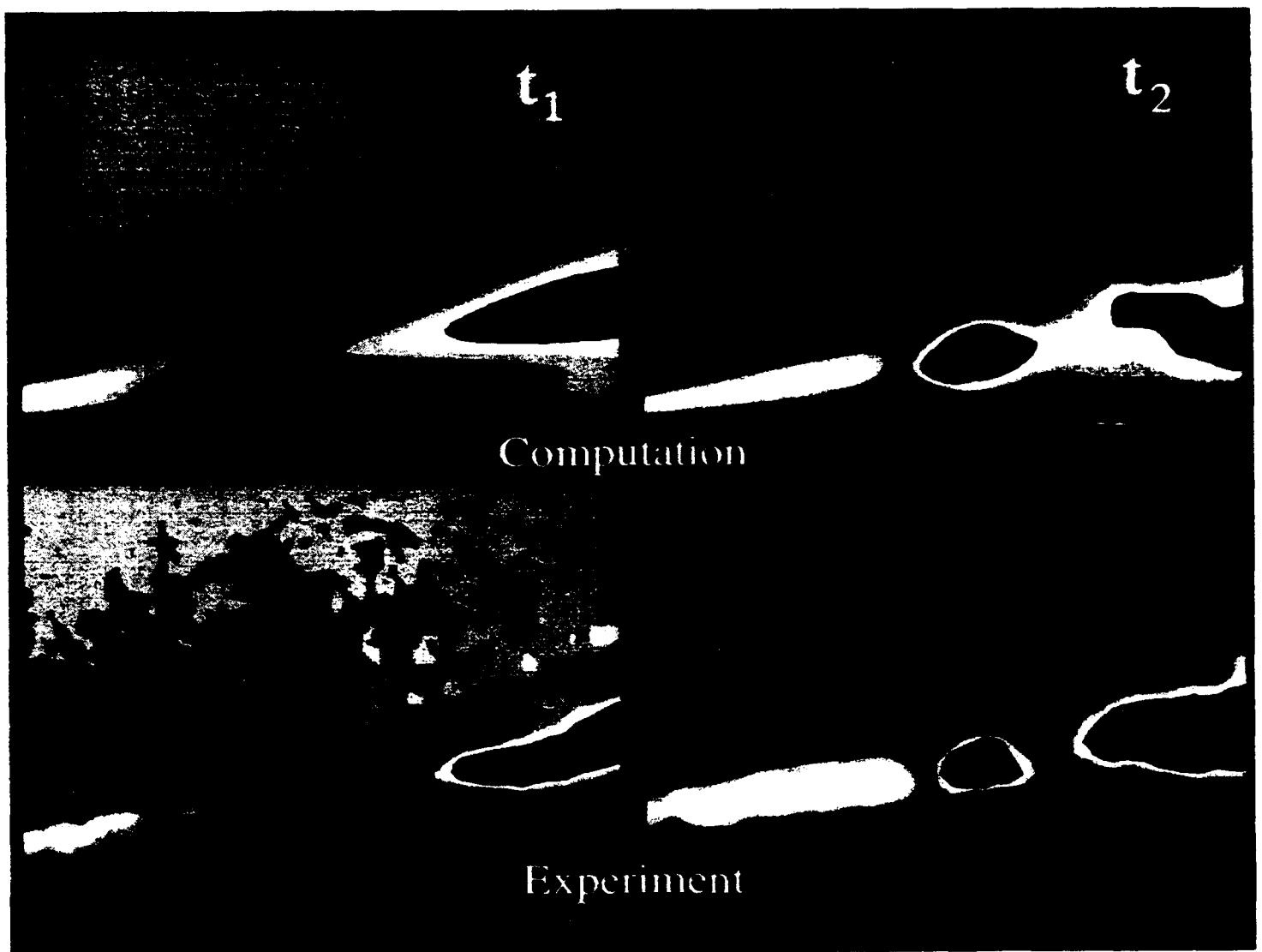


Figure 9: Comparison of Computed and Experimental [19] Axial Velocity Contours on Plane Through Vortex Core

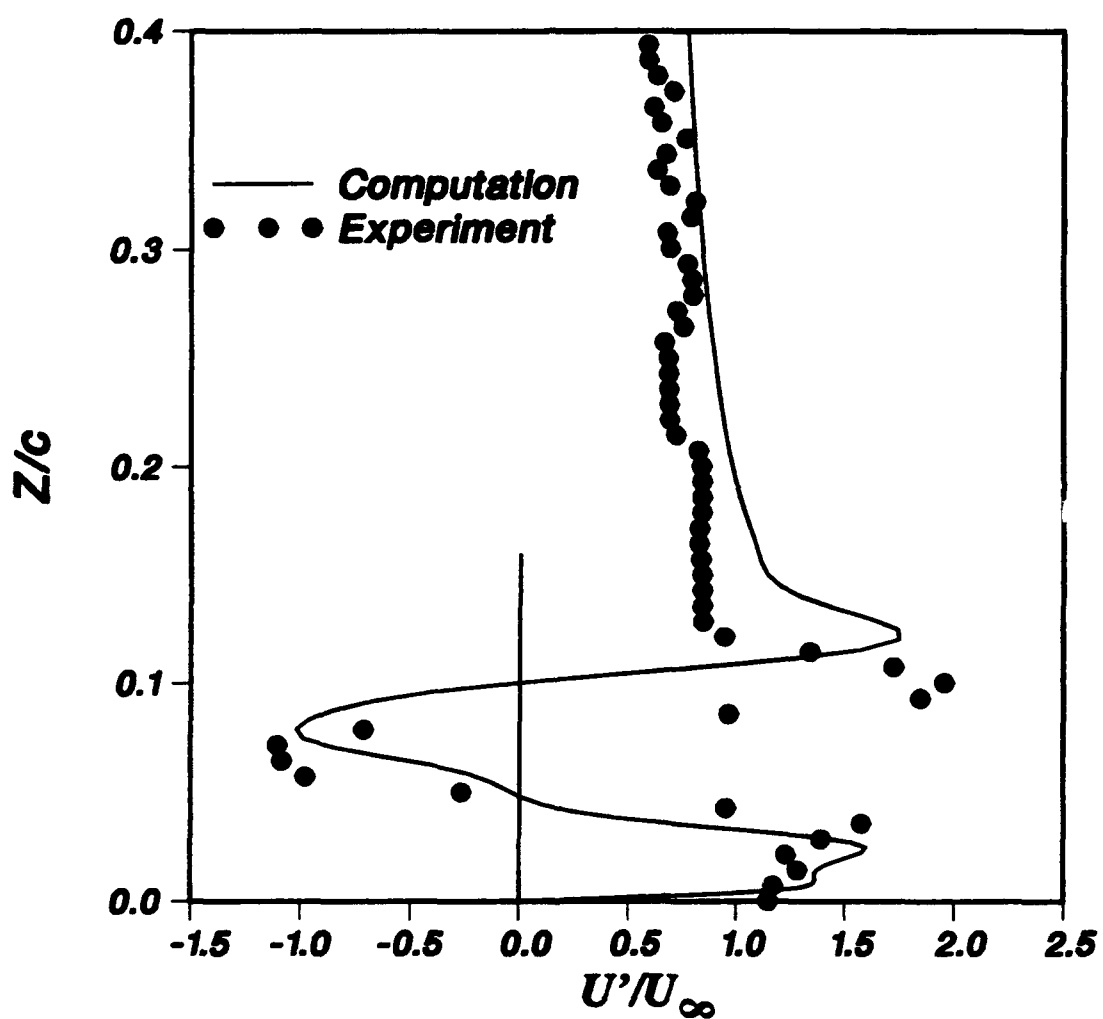
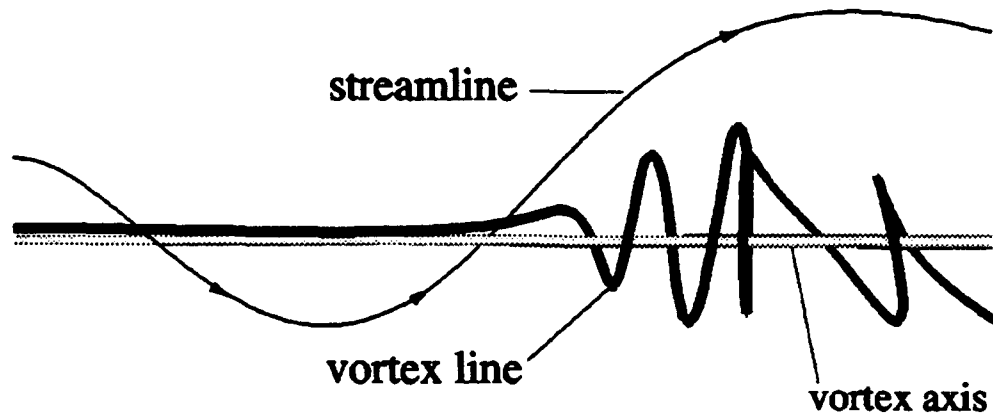
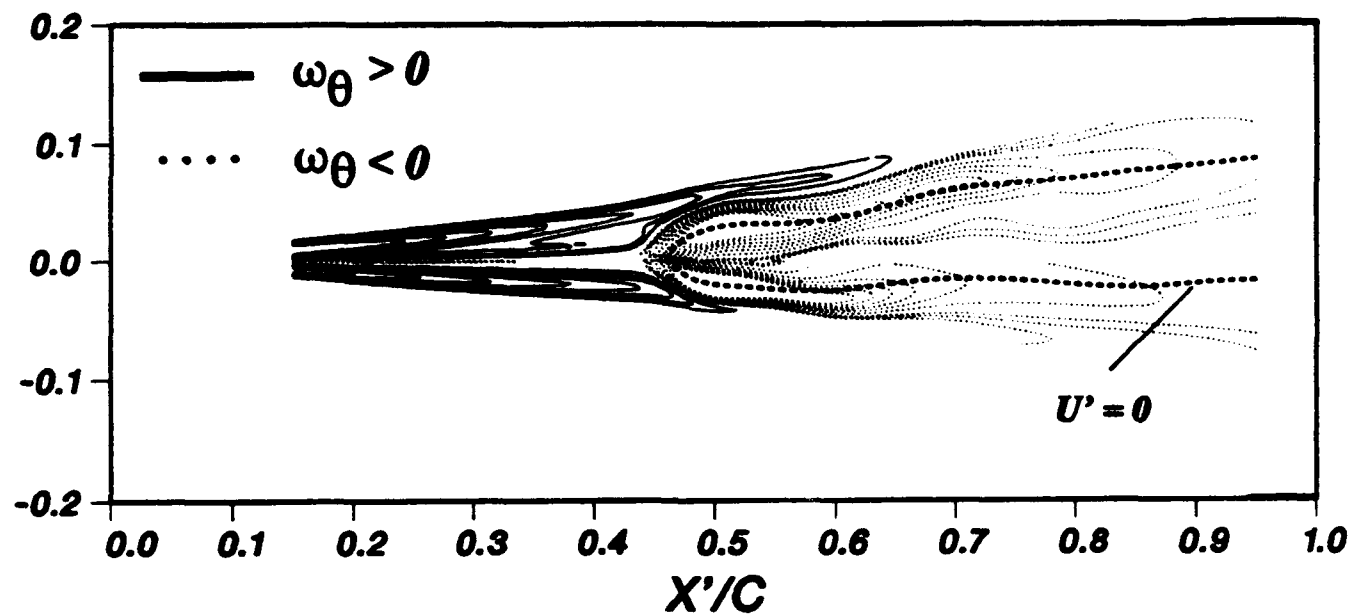


Figure 10: Comparison of Computed and Experimental [19] Axial Velocity Profiles Through Breakdown Bubble



(b)

Figure 11: Switch of Azimuthal Vorticity Component, $t^+ = 2.26$

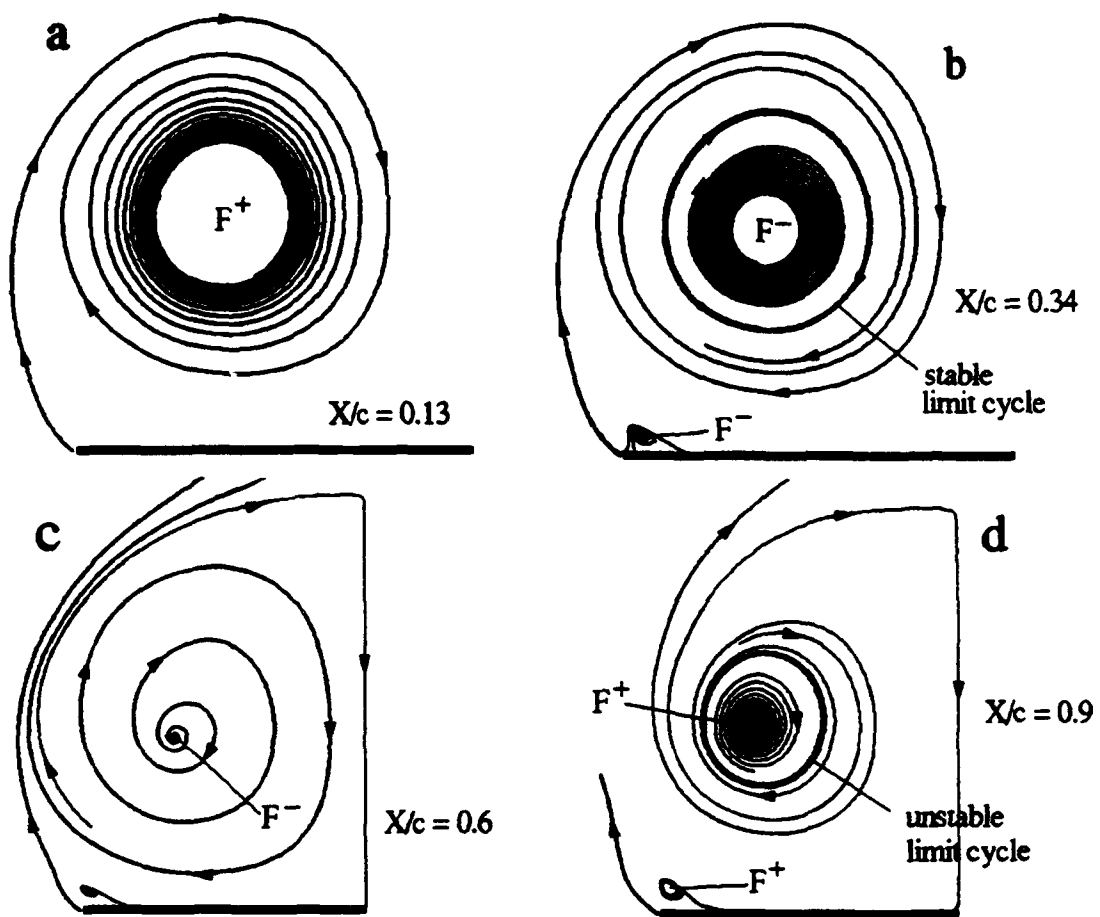


Figure 12: Evolution of Crossflow Topology, $t^+ = 2.06$

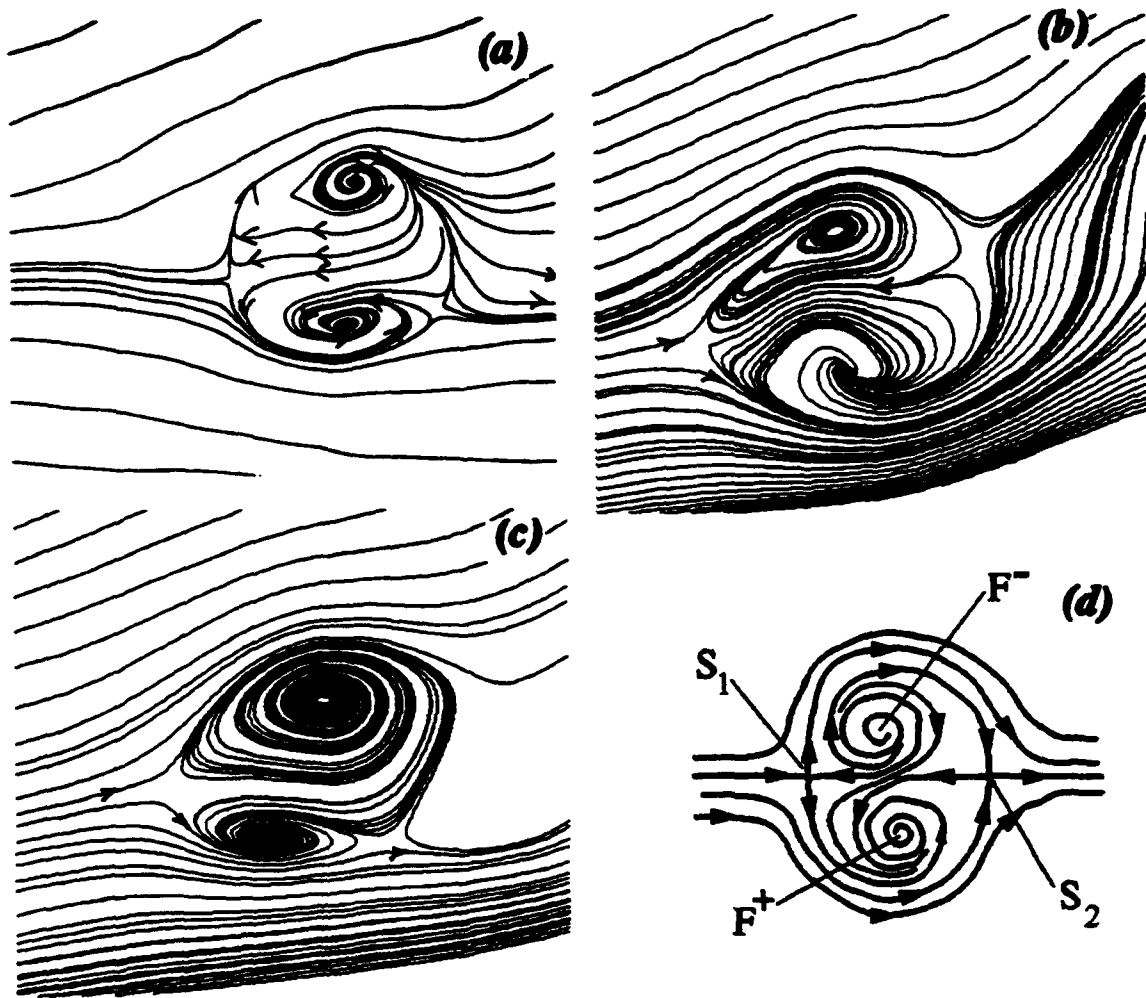


Figure 13: Sectional Streamline Patterns on Vertical Plane Through Breakdown Bubble:
 (a) Experiment [19], (b) Computed, $t^+ = 2.4$, (c) Computed, $t^+ = 2.6$, (d) Schematic

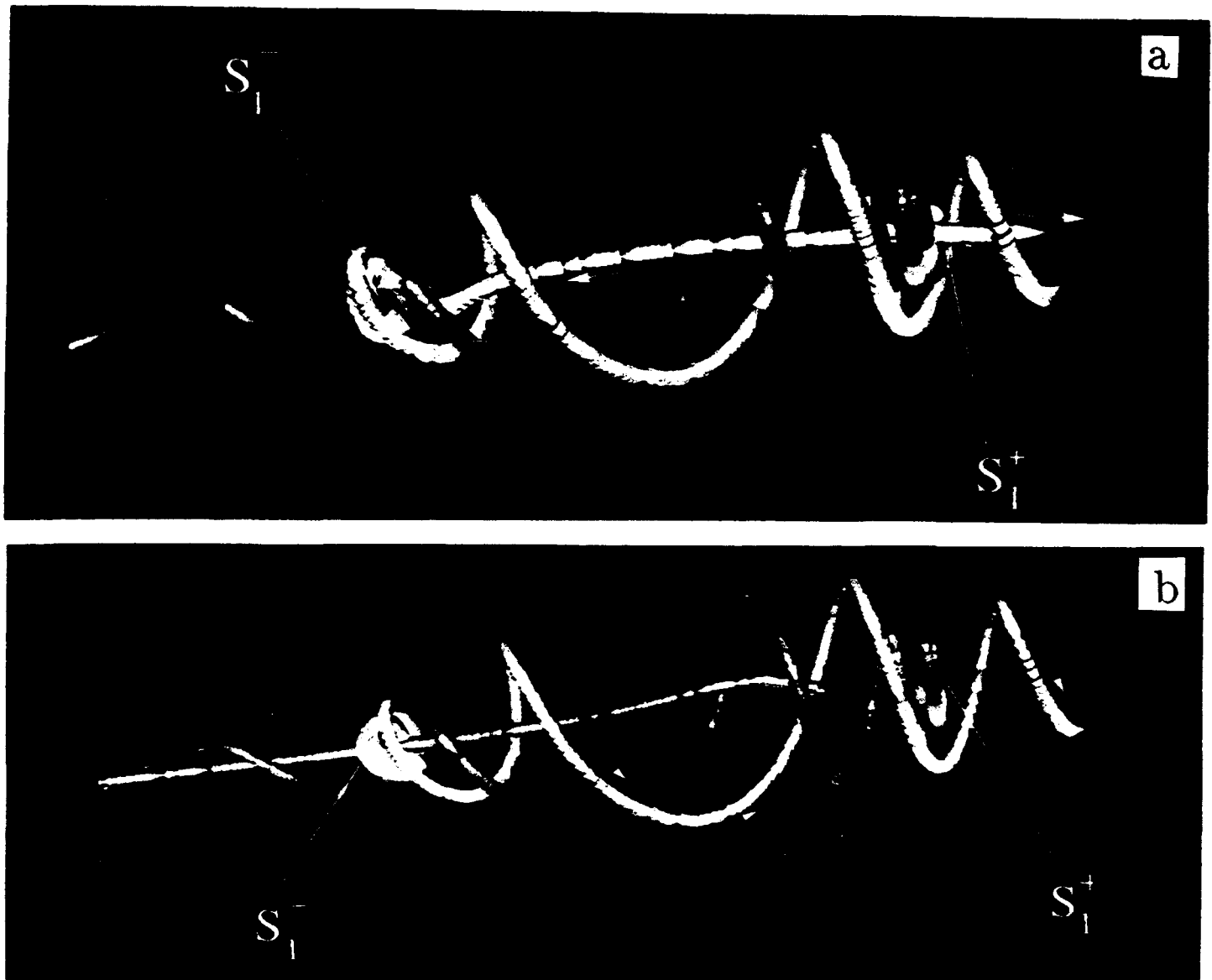


Figure 14: Three Dimensional Critical Points and Trajectories in Vortex Breakdown Region
at $t^+ = 1.8$

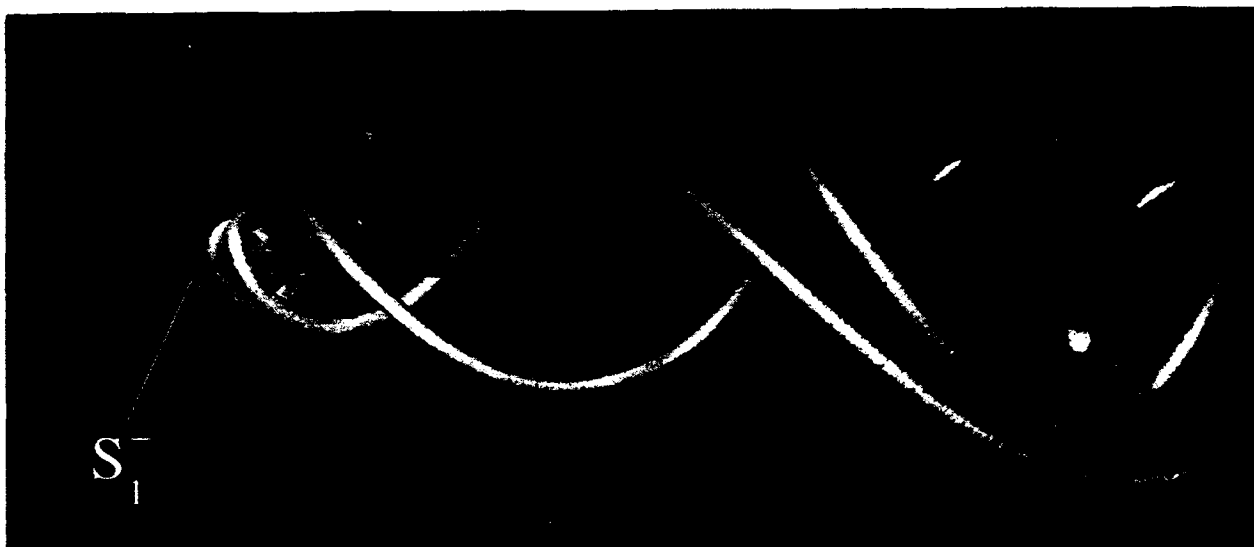
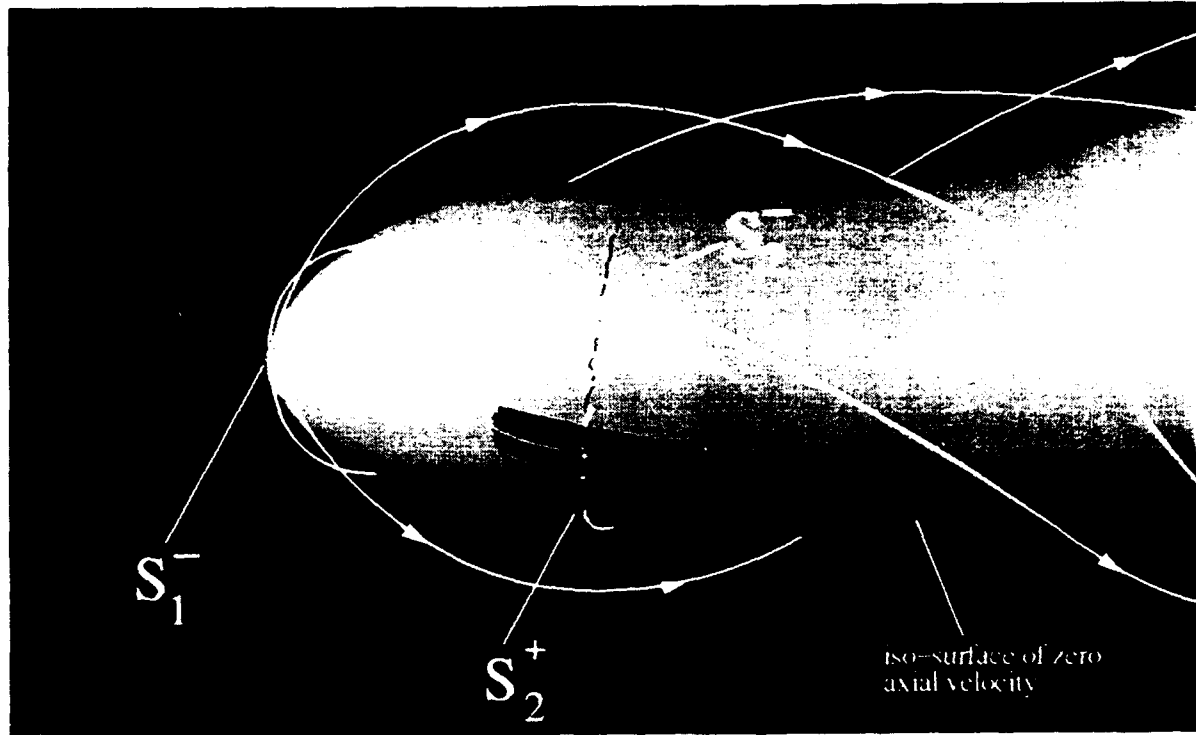
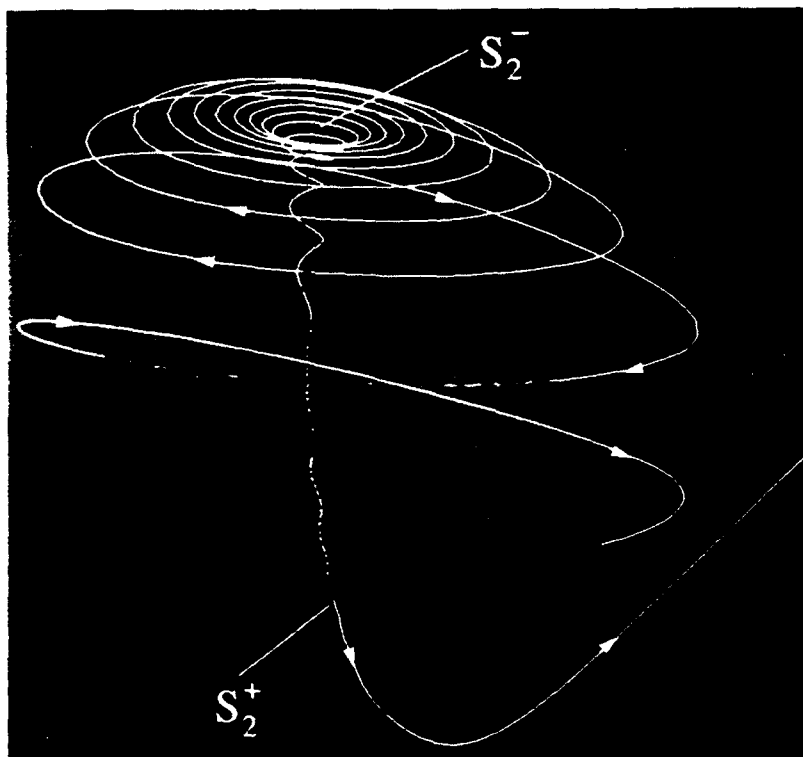


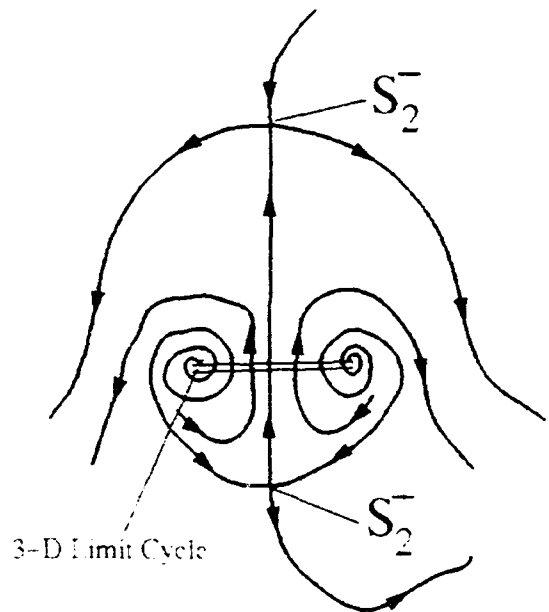
Figure 15: Three Dimensional Critical Points and Trajectories in Vortex Breakdown Region at $t^+ = 2.06$



a



b



c

Figure 16: Three Dimensional Critical Points and Trajectories in Vortex Breakdown Region at $t^+ = 2.26$

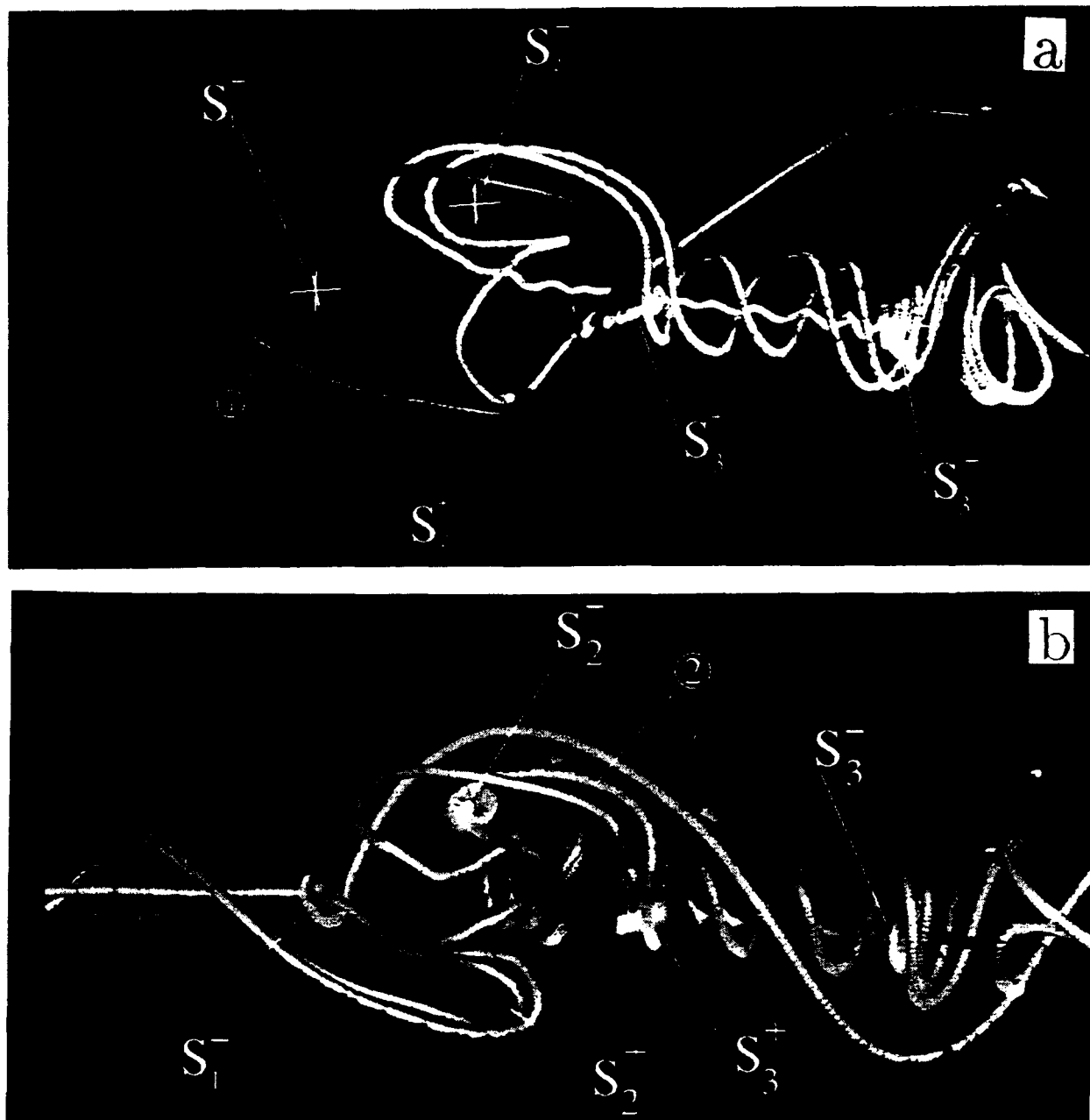


Figure 17: Three Dimensional Critical Points and Trajectories in Vortex Breakdown Region at $t^+ = 2.4$

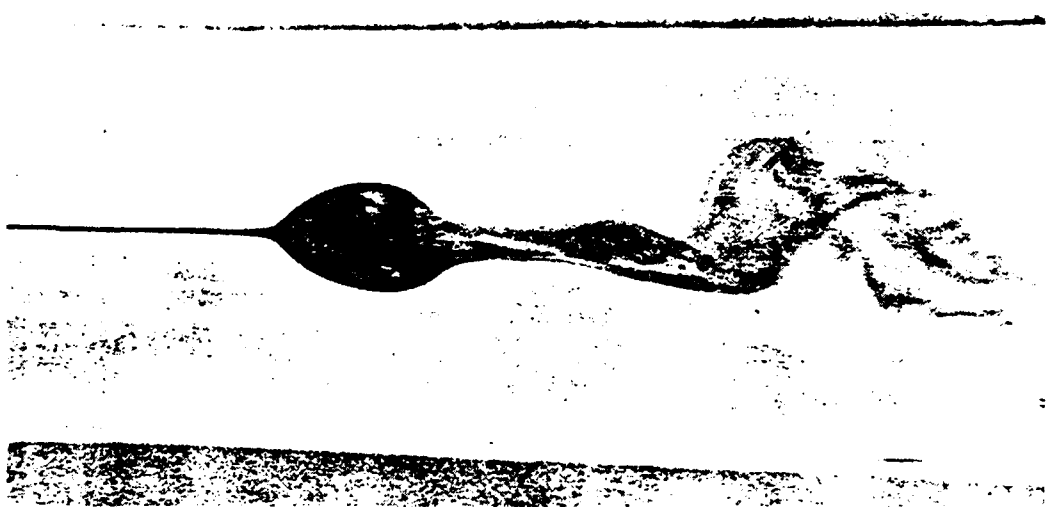
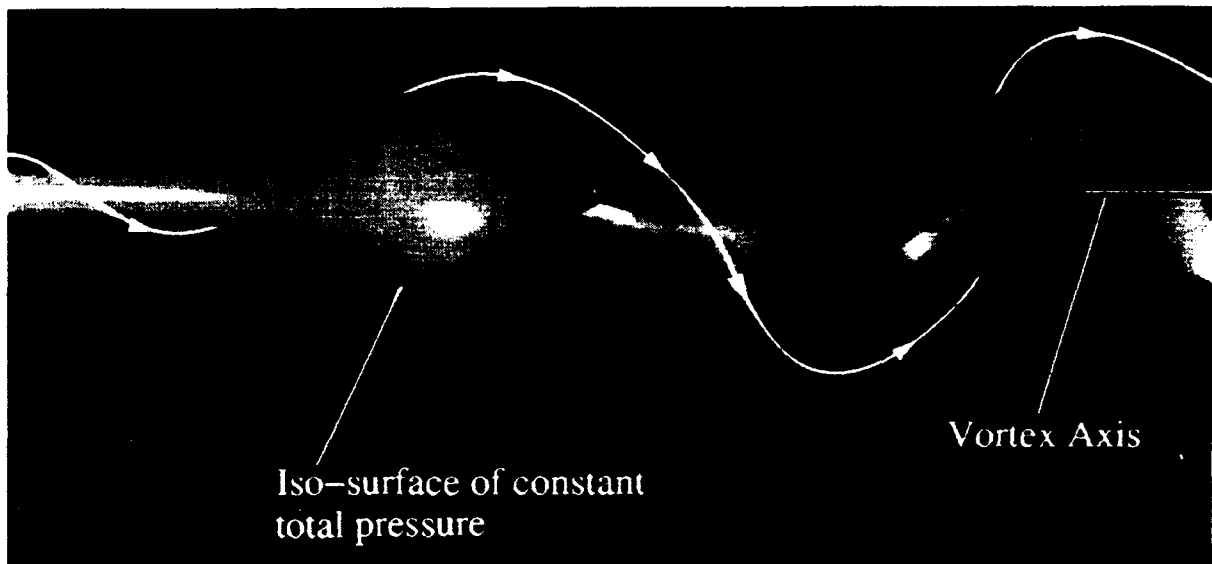


Figure 18: Comparison of Computed Results with Experimental [13] Flow Visualization of 'Axisymmetric' Vortex Breakdown in a Tube